Estimation of Disturbance Inputs to a Tire Coupled Quarter-car Suspension Test Rig

by

Jonathan Daniel Ziegenmeyer

Thesis submitted to the Faculty of the

Virginia Polytechnic Institute and State University

in partial fulfillment of the requirements for the degree of

Master of Science

in

Mechanical Engineering

Approved:

Steve Southward, Chairman

Mehdi Ahmadian

John Ferris

Corina Sandu

May 8, 2007
Blacksburg, Virginia

Keywords: real-time, open loop, quarter-car, suspension, disturbance estimation

Estimation of Disturbance Inputs to a Tire Coupled Quarter-car Suspension Test Rig

by

Jonathan Daniel Ziegenmeyer

Steve Southward, Chairman
Mechanical Engineering

ABSTRACT

In this study a real-time open loop estimate of the disturbance displacement input to the tire and an external disturbance force, representing handling and aerodynamic forces, acting on the sprung mass of a quarter-car suspension test rig was generated. This information is intended for use in active control methods applied to vehicle suspensions. This estimate is achieved with two acceleration measurements as inputs to the estimator; one each on the sprung and unsprung masses. This method is differentiated from current disturbance accommodating control, bilinear observers, and preview control methods. A description of the quarter-car model and the experimental test rig is given.

The equations of motion for the quarter-car model are derived in state space as well as a transfer function form. Several tests were run in simulation to investigate the performance of three integration techniques used in the estimator. These tests were first completed in continuous time prior to transforming to discrete time. Comparisons are made between the simulated and estimated displacement and velocity of the disturbance input to the tire and disturbance force input to the sprung mass. The simulated and estimated dynamic tire normal forces are also compared. This process was necessary to select preliminary values for the integrator transfer function to be implemented in real-time.

Using the acceleration measurements from the quarter-car test rig, a quarter-car parameter optimization for use in the estimator was performed. The measured and estimated tire disturbance input, disturbance input velocity, and dynamic tire normal force signals are compared during experimental tests. The results show that the open loop observer provides estimates of the tire disturbance velocity and dynamic tire normal force with acceptable error. The results also indicate the quarter-car test rig behaves linearly within the frequency range and amplitude of the disturbance involved in this study. The resultant access to the disturbance estimate and dynamic tire force estimate in real-time enables pursuit of novel control methods applied to active vibration control of vehicle suspensions.

CONTENTS

NOMECLATURE

m_s	sprung mass
m_u	unsprung mass
k_s	suspension stiffness
k_u	unsprung mass (tire) stiffness
b_s	suspension damping coefficient
b_u	unsprung mass (tire) damping coefficient
b_{sf}	linear bearing damping coefficient
w	time-varying disturbance input to tire contact patch
F_c	time-varying control force
F_d	time-varying disturbance force affecting sprung mass
F_s	time-varying suspension force
F_t	time-varying tire force
s	Laplace operator

$\mathbf{A}, \mathbf{B}, \mathbf{C}, \mathbf{D}, \mathbf{E}, \mathbf{F}$	state space matrices
Z_u	mechanical impedance of tire
Z_s	mechanical impedance of suspension
$\mathbf{x}$	state vector
$\mathbf{y}$	state space output vector
$\mathbf{u}$	state space control vector
a_s	acceleration of sprung mass
a_u	acceleration of unsprung mass
ζ	damping ratio of filter transfer functions
t_s	sample time
$\mathbf{e}$	error vector for r.m.s. calculations
$\mathbf{p}$	measurement vector for r.m.s. calculations

LIST OF TABLES

LIST OF FIGURES

1 INTRODUCTION

This chapter begins by describing the motivation for this study. The objectives of the study are presented next. The chapter ends with an outline for the remainder of the thesis.

1.1 Motivation

The quarter-car model of a vehicle suspension has been extensively studied in relation to active vibration control [21]. These models are generally used due to their simplicity and pertinent results to examine the ride and handling characteristics of a vehicle. Many of these models incorporate a state estimator or observer since it is otherwise expensive or impractical and in some cases impossible to obtain dynamic information about interesting states of the suspension while the vehicle is in motion.

For example, dynamic tire normal force of a rolling tire may be of interest. One way to obtain this information is demonstrated in [11] where strain gauges are mounted on the spindle and accelerometers on the upright of a heavy truck suspension. Another way to measure this force is through specially instrumented wheels that can measure three forces and three moments about the local wheel coordinate system [12]. These wheels are impractical for use as standard equipment for vehicles due to their high cost. It will be shown in this study that the dynamic tire normal force of a stationary tire on a flat plate can be estimated using only two accelerometers which are more robust and relatively inexpensive compared to these other sensing methods mentioned. This is the seminal step in the development of a viable active control algorithm.

In order to estimate the tire normal force, the input to the tire needs to be known or estimated. Many methods exist for obtaining this information such as directly measuring the road profile. The direct measurement methods which provide a point mapping of the road profile across the width of the road are of little interest for this study since the amount of data involved is too cumbersome for real-time use. Furthermore, the test rig

involved in this study lacks the ability to represent a non-uniform surface under the tire contact patch, therefore the enveloping properties of a tire are not considered.

Optical look-ahead preview sensors measure the reflection of a laser beam projected a distance ahead of the tire contact patch. These sensors are quite expensive and a reasonable estimate of the road disturbance for use in real-time control can be obtained from less expensive and simpler sensors. This claim will be demonstrated in this study.

1.2 Objectives

The first objective of this study was to estimate, via linear control methods, the disturbance inputs to a quarter-car simulation model. The second objective was to apply the developed observer in real-time to the tire coupled quarter-car suspension test rig at the Performance Engineering Research Lab (PERL) at Virginia Tech/IALR. The resultant access to the disturbance estimate and subsequent dynamic tire force estimate in real-time enables pursuit of novel control methods applied to active vibration control of vehicle suspensions. Achieving these objectives will contribute to the knowledge base of the Performance Engineering Research Laboratory and provide a direction for further study.

1.3 Outline

The remainder of this thesis begins with a literature review on observers applied to vehicle suspension, tire disturbance measurement and estimation, and look-ahead preview control. Chapter 3 is a discussion of the control theory involved in this study, specifically quarter-car models, disturbance accommodating control, and an open loop observer. Chapter 4 presents the application of the quarter-car models and open loop observer to simulations performed in Matlab/Simulink. The subsequent results and a description of the experimental test rig are also presented. Chapter 5 describes the experimental procedures and explains the results of the experimental tests. This thesis closes with conclusions and some recommendations for further study in chapter 6.

2 LITERATURE REVIEW

This chapter presents the results of a search for previous literature written in the areas of tire disturbance measurement and estimation, look-ahead preview control, and observers applied to suspension systems. How the present study differs from these areas is also explained in this chapter.

2.1 Tire disturbance measurement and estimation

Two methods for directly measuring a road profile are via a profilometer and a longitudinal profile analyzer. A profilometer measures acceleration of the sprung mass of the vehicle on which it is mounted. This acceleration is double integrated resulting in a displacement which is compared to an acoustic or optical measurement of the distance between the accelerometer and the road. The road profile is obtained by subtracting the two signals [7].

A longitudinal profile analyzer is a trailer comprised of a ballast beam suspended by a swing arm which is towed behind a vehicle. The road profile is obtained by measuring the relative angle between the swing arm and the beam. The road considered in [7] is without bumps. A phase distortion correction has to be performed to obtain reliable information from rough roads. A comparison between the estimate of the road profile obtained by a sliding mode observer applied to a full vehicle model and the profile measured by a longitudinal profile analyzer indicates the estimate is a good representation of the measured road profile [7]. In this study a simpler open loop observer is derived from a quarter-car model to estimate the road disturbance. Furthermore, this estimate will be used for real-time applications and must not be misinterpreted as a method for obtaining the road information necessary for chassis durability studies.

Response type road profiling systems are based on measured vehicle responses to road inputs, such as accelerations. The vehicle dynamics of the specific vehicle used to obtain

the responses are implicit in this type of characterization. An effective road profile may be developed in post processing from this data by use of a model, but the application of the data is restricted to the vehicle on which it was measured and relies heavily on the fidelity of the vehicle and tire model from which it was obtained. [23]

These methods are not practical for real-time controls applications where interest is focused on the current disturbance input to the system. One of the intentions of this thesis is to provide a real-time estimate of the disturbance input to the tire, not to acquire knowledge about roads for use in any other study.

2.2 Look-ahead preview control

The pioneering research in the area of look-ahead preview information applied to vehicle suspension control was developed by Bender [2]. He proposed the use of preview information to eliminate the compromise between vibration and clearance space in control design. His single degree of freedom quarter-car model indicated substantial gains could be had in improving the ride quality if preview information was available.

Generally, two methods exist for obtaining preview information. These are direct measurement of the road some distance in front of the axle via look-ahead sensors and reconstruction of the road profile from suspension measurements of an axle. If preview information is based on look-ahead sensors then both axles can be controlled, but these sensors show a pile of leaves as a major disturbance while a pothole filled with water appears smooth. If preview information is obtained from the measurements of the front axle it may be used to control the rear axle since the rear should encounter the same disturbances as the front except at a time delay which is a function of the vehicle speed and wheelbase. Inaccuracies with this method are exemplified by the front and rear axle paths around a turn differing enough such that the rear axle does not encounter the same disturbances as the front. Furthermore, an obstruction such as a stone could be pushed by the front axle out of the path of the rear axle [14].

Gordon and Sharp [1] concluded preview information shows the most benefit when applied to controlling the unsprung mass. It was also demonstrated that a preview time

greater than 0.1s is not advantageous. These preview sensors are lasers mounted on the chassis and usually have a fixed preview length. Since this length is fixed, the amount of time between the sensed road irregularity and that irregularity affecting the suspension decreases with increasing vehicle speed.

Using a technique known as step-ahead or multi-step ahead prediction, it is possible to use the estimation of the disturbances to gain a priori information about the disturbances. This a priori information can be used for active suspension control applications in a similar fashion to the information from look-ahead sensors. Step-ahead prediction refers to the ability to estimate the disturbance one or several discrete time steps into the future based on the current and past measurements. For a fundamental description of step-ahead prediction, the reader is encouraged to read [15, 16, 17, 18, 19].

2.3 Observers applied to suspension systems

A classical observer requires that all dynamic system inputs be known or measurable. Therefore, it is not capable of dealing with unknown or immeasurable disturbances and must be supplemented to account for the disturbances. One solution to this problem is disturbance accommodating control or DAC in which the classical observer is augmented with a state space representation of the disturbance.

Disturbance accommodating control was proposed by Johnson [8] as a method of dealing with system inputs which are unknown. These inputs can be comprised of transient and/or steady state components. With this technique, modeling errors of system parameters or state dependencies which lead to poor performance can be treated as an unknown disturbance. For example, a DAC method was developed in [6] that forces a system with coupling and nonlinear terms to behave like a reduced order model. The differences between the original system and the reduced order model are treated as disturbances.

Disturbances are classified as either noise-type or having waveform structure. Waveform disturbances can be described by a linear combination of weighted basis functions whose weighting coefficients are unknown and may change in a random manner. The

disturbance input to a vehicle model does not behave like a noise-type disturbance since it is not completely erratic and displays some waveform structure.

A second method discussed is the construction of a bilinear observer. Hac [3] claims linear observers are difficult to apply to bilinear systems with unknown inputs, such as quarter-car models, because these observers require prior knowledge about the disturbance and involve a lengthy on-line iterative process. He assumes that the sprung mass displacement relative to the road, the unsprung mass velocity and the suspension deflection are measured. Hedrick et al [4] construct a bilinear observer that supplies state estimates regardless of the unknown disturbance input velocity and in the presence of parametric and modeling errors of the quarter-car model. A continuation of this work by Yi [5] shows the observer estimation error is independent of the unknown disturbance. All states are estimated in [5] using only sprung and unsprung mass accelerometer signals. Velocities are obtained by pseudo-integrating the acceleration measurements and are estimated without the effects of DC offsets.

The observer developed in this study is a more straightforward technique for estimating and accounting for the disturbances. This study also presents how a disturbance force input to the sprung mass due to handling and/or aerodynamic forces can be estimated.

3 CONTROL THEORY

This section begins with a discussion of various quarter-car suspension models. After the chosen model is explained, the equations of motion are developed in state space form and in transfer function form. The type of linear estimator considered, an open loop observer, is then presented. Concluding this chapter is a discussion of a parameter optimization method applied to an open loop observer.

3.1 Plant models

The purpose of a quarter-car model is to simplify the complexities of the nonlinear dynamics of a full vehicle while providing meaningful results. With regards to the seminal aspect of this study, it is logical to use a linear quarter-car model to represent the behavior of one corner of the vehicle under the considered disturbances.

The simplest quarter-car model is a single lumped mass, representing a quarter of the mass of the vehicle, connected to the road via a linear spring and damper in parallel, representing the primary suspension. This type of model neglects the unsprung mass and its associated stiffness and damping characteristics. The majority of quarter-car models used for active vibration studies are similar to Figure 3-1 where the sprung and unsprung masses of the vehicle are represented by lumped masses and the tire is represented by a spring between the unsprung mass and the road. The inclusion of a damper in parallel with this spring is a more accurate representation of the tire dynamics [20]. Both these elements modeling the tire are assumed linear in this study.

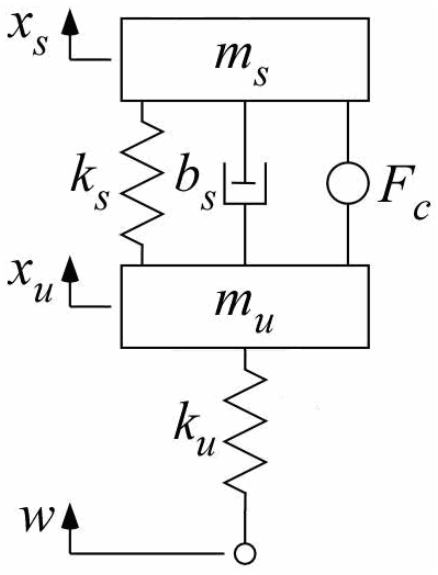

Figure 3-1 Typical quarter-car model with active element

The model used in this study is shown in Figure 3-2. Since there was no active element implemented in this study, the control force F_c is set to zero although this term is carried through the calculations. The quarter-car test rig used in this study was developed such that an external force could be applied to the sprung mass via linear motors. This force, F_d, could be due to a combination of handling and aerodynamic forces acting on an actual vehicle and is treated as an unknown disturbance. The linear motors were not installed at the time of this study; therefore the disturbance force will be comprised of only the force due to the friction in linear guides which constrain the sprung mass of the rig. The friction will be treated as linear viscous damping.

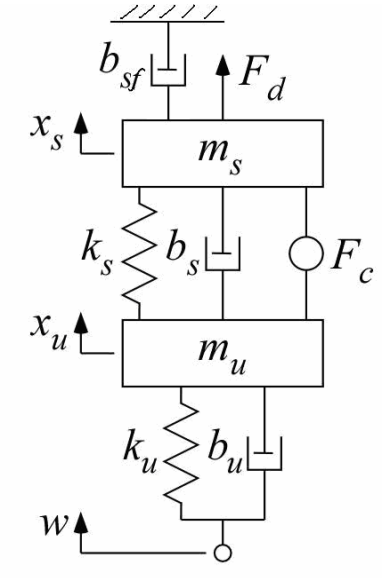

Figure 3-2 Disturbed quarter-car model of this study

The preliminary values for the sprung and unsprung mass parameters were determined from the readings of setup scales supporting a typical road course prepared Porsche 911 (996). The unsprung mass consisted of the wheel, upright, brake rotor and caliper, and half of the strut and control arms. The mass of the sum of these components was known with reasonable accuracy which enabled the determination of the sprung mass value. The springs and dampers are assumed to be linear elements.

3.1.1 Equations of motion in time domain

A force balance performed on the sprung mass of Figure 3-2 yields

$$m_s\ddot{x}_s = -\left(b_s + b_{sf}\right)\dot{x}_s - k_s x_s + b_s\dot{x}_u + k_s x_u + F_d + F_c \qquad \text{Eq. 3.1}$$

A force balance on the unsprung mass results in

$$m_u\ddot{x}_u = -b_s\dot{x}_u - k_s x_u + b_s\dot{x}_s + k_s x_s - F_c + b_u\dot{w} + k_u w - b_u\dot{x}_u - k_u x_u \qquad \text{Eq. 3.2}$$

These equations are combined into a state space form with state vector $\mathbf{x} = \begin{bmatrix} \dot{x}_s & \ddot{x}_s & \dot{x}_u & \ddot{x}_u & \dot{w} \end{bmatrix}^T$ as

$$\dot{\mathbf{x}} = \mathbf{Ax} + \mathbf{Bu} + \mathbf{F}\begin{bmatrix} F_d \\ \dot{w} \end{bmatrix}$$
$$\mathbf{y} = \mathbf{Cx} + \mathbf{Du} + \mathbf{E}\begin{bmatrix} F_d \\ \dot{w} \end{bmatrix} \qquad \text{Eq. 3.3}$$

The output vector is $\mathbf{y} = \begin{bmatrix} \ddot{x}_s & \ddot{x}_u & x_s & \dot{x}_s & x_u & \dot{x}_u & w & F_t & F_s \end{bmatrix}^T$. The definitions of the A, B, C, D, E, and F matrices can be found in the Appendix.

3.1.2 Transfer function form of equations of motion

The sprung and unsprung mass force balance equations can be expressed in the frequency domain as

$$\left(m_s s^2 + \left(b_s + b_{sf}\right)s + k_s\right)x_s = \left(b_s s + k_s\right)x_u + F_d + F_c \qquad \text{Eq. 3.4}$$

$$\left(m_u s^2 + \left(b_u + b_s\right)s + \left(k_u + k_s\right)\right)x_u = \left(b_u s + k_u\right)w + \left(b_s s + k_s\right)x_s - F_c \qquad \text{Eq. 3.5}$$

Introducing the concept of mechanical impedance, symbolized by a capital Z, the damping and spring terms can be represented in the frequency domain as

$$Z_s = b_s s + k_s$$
$$Z_u = b_u s + k_u \qquad \text{Eq. 3.6}$$

To further simplify the equations the following terms are defined

$$\Delta_s = m_s s^2 + b_{sf} + Z_s$$
$$\Delta_u = m_u s^2 + Z_u \qquad \text{Eq. 3.7}$$
$$\Delta = \Delta_s\left(\Delta_u + Z_s\right) - Z_s^2$$

Applying equations 3.6 and 3.7 to the force balance equations results in the matrix representation

$$\begin{bmatrix} \Delta_s & -Z_s \\ -Z_s & (\Delta_u + Z_s) \end{bmatrix} \begin{bmatrix} x_s \\ x_u \end{bmatrix} = \begin{bmatrix} 1 & 1 & 0 \\ -1 & 0 & Z_u \end{bmatrix} \begin{bmatrix} F_c \\ F_d \\ w \end{bmatrix} \qquad \text{Eq. 3.8}$$

Solving for $\begin{bmatrix} x_s & x_u \end{bmatrix}^T$ yields

$$\begin{bmatrix} x_s \\ x_u \end{bmatrix} = \left(\frac{1}{\Delta}\right) \begin{bmatrix} \Delta_u & (\Delta_u + Z_s) & Z_s Z_u \\ (Z_s - \Delta_s) & Z_s & \Delta_s Z_u \end{bmatrix} \begin{bmatrix} F_c \\ F_d \\ w \end{bmatrix}$$

$$\begin{bmatrix} x_s \\ x_u \end{bmatrix} = \begin{bmatrix} P_{sc} & P_{sd} & P_{sw} \\ P_{uc} & P_{ud} & P_{uw} \end{bmatrix} \begin{bmatrix} F_c \\ F_d \\ w \end{bmatrix} \qquad \text{Eq. 3.9}$$

Equation 3.9 results in transfer functions between the sprung and unsprung mass displacement and the control force, disturbance force, and disturbance displacement. The six transfer functions are expanded as

$$P_{sc} = \left(\frac{\Delta_u}{\Delta}\right) = \left(\frac{m_u s^2 + b_u s + k_u}{m_s m_u s^4 + \left(m_u\left(Z_s + b_{sf}\right) + m_s\left(Z_s + Z_u\right)\right)s^2 + Z_s Z_u + b_{sf}\left(Z_s + Z_u\right)}\right)$$

$$P_{uc} = \left(\frac{-m_s s^2}{\Delta}\right) = \left(\frac{-m_s s^2}{m_s m_u s^4 + \left(m_u\left(Z_s + b_{sf}\right) + m_s\left(Z_s + Z_u\right)\right)s^2 + Z_s Z_u + b_{sf}\left(Z_s + Z_u\right)}\right)$$

$$P_{sd} = \left(\frac{\Delta_u + Z_s}{\Delta}\right) = \left(\frac{m_u s^2 + \left(b_u + b_s\right)s + \left(k_u + k_s\right)}{m_s m_u s^4 + \left(m_u\left(Z_s + b_{sf}\right) + m_s\left(Z_s + Z_u\right)\right)s^2 + Z_s Z_u + b_{sf}\left(Z_s + Z_u\right)}\right)$$

$$P_{ud} = \left(\frac{Z_s}{\Delta}\right) = \left(\frac{b_s s + k_s}{m_s m_u s^4 + \left(m_u\left(Z_s + b_{sf}\right) + m_s\left(Z_s + Z_u\right)\right)s^2 + Z_s Z_u + b_{sf}\left(Z_s + Z_u\right)}\right)$$

$$P_{sw} = \left(\frac{Z_s Z_u}{\Delta}\right) = \left(\frac{\left(b_s s + k_s\right)\left(b_u s + k_u\right)}{m_s m_u s^4 + \left(m_u\left(Z_s + b_{sf}\right) + m_s\left(Z_s + Z_u\right)\right)s^2 + Z_s Z_u + b_{sf}\left(Z_s + Z_u\right)}\right)$$

$$P_{uw} = \left(\frac{\Delta_s Z_u}{\Delta}\right) = \left(\frac{\left(m_s s^2 + \left(b_s + b_{sf}\right)s + k_s\right)\left(b_u s + k_u\right)}{m_s m_u s^4 + \left(m_u\left(Z_s + b_{sf}\right) + m_s\left(Z_s + Z_u\right)\right)s^2 + Z_s Z_u + b_{sf}\left(Z_s + Z_u\right)}\right)$$

These transfer functions are all proper, i.e. the number of poles is greater than or equal to the number of zeros. It should be noted that in practice the output signals are not displacement but rather acceleration measurements. Defining the sprung and unsprung mass accelerations as a_s and a_u and substituting into equation 3.9 yields

$$\begin{bmatrix} a_s \\ a_u \end{bmatrix} = s^2 \begin{bmatrix} x_s \\ x_u \end{bmatrix} = s^2 \begin{bmatrix} P_{sc} & P_{sd} & P_{sw} \\ P_{uc} & P_{ud} & P_{uw} \end{bmatrix} \begin{bmatrix} F_c \\ F_d \\ w \end{bmatrix} \qquad \text{Eq. 3.10}$$

While all the other transfer functions remain proper, this procedure causes the transfer function between the unsprung acceleration and the disturbance displacement P_{uw} to become improper. The numerator becomes fifth order while the denominator is fourth order. Two methods exist for solving this problem. The first is to assume that velocities are measured instead of accelerations. The second method is to assume that the disturbance is a velocity instead of a displacement. Applying the latter technique to equation 3.10 yields

$$\begin{bmatrix} a_s \\ a_u \end{bmatrix} = s^2 \begin{bmatrix} P_{sc} & P_{sd} & P_{sw} \\ P_{uc} & P_{ud} & P_{uw} \end{bmatrix} \begin{bmatrix} F_c \\ F_d \\ \frac{\dot{w}}{s} \end{bmatrix} = \begin{bmatrix} s^2 P_{sc} & s^2 P_{sd} & s P_{sw} \\ s^2 P_{uc} & s^2 P_{ud} & s P_{uw} \end{bmatrix} \begin{bmatrix} F_c \\ F_d \\ \dot{w} \end{bmatrix} \qquad \text{Eq. 3.11}$$

3.1.3 Block diagram model

There are many different techniques available for generating the equations of motion for a quarter-car model. In order to have a more visual representation, a block diagram quarter-car model was developed to view the signal paths and generate insight to the explicit signal flows. Figure 3-3 shows the three inputs to the model which are the control and disturbance forces and the disturbance input to the tire. The gain blocks represent the quarter-car spring, mass and damping parameters. The gray *goto* blocks enable the user to define the output of the model as acceleration, velocity, or displacement of the masses. It should be noted that this is a continuous time model.

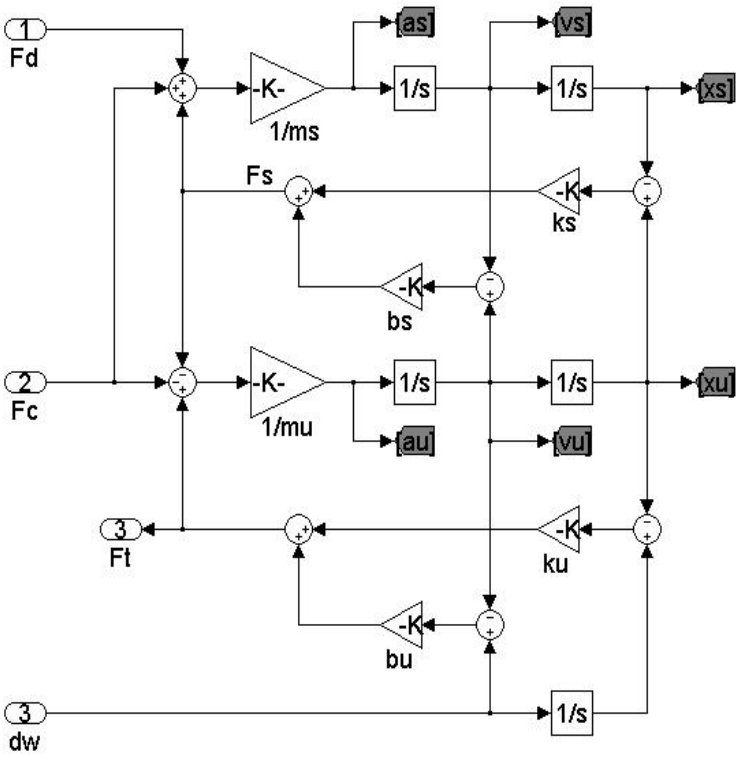

Figure 3-3 Block diagram version of quarter-car model

3.2 Open loop estimator

Several methods of state estimation have been developed and applied to vehicle control, the most straightforward of which is an open loop observer. In this study an open loop observer was developed that is somewhat of an inverse model of the plant in that the acceleration signals are used as inputs to estimate the disturbance displacement input to the tire and sprung mass disturbance force. In contrast, the plant inputs are the disturbances and its outputs are measured acceleration signals. Using the previously developed equations of motion in the frequency domain from section 3.1.2, the desired estimator outputs can be calculated. The suspension force can be represented as

$$F_s = b_s\dot{x}_u - b_s\dot{x}_s + k_s x_u - k_s x_s = \frac{1}{s^2} Z_s \left(a_u - a_s\right) \qquad \text{Eq. 3.12}$$

Substituting this into the equation of motion for the sprung mass and solving for the disturbance force yields

$$F_d = m_s a_s s^2 + b_{sf} x_s s - F_s - F_c \qquad \text{Eq. 3.13}$$

The dynamic tire force can be represented as

$$F_t = b_u \dot{w} + k_u w - b_u \dot{x}_u - k_u x_u = Z_u \left(w - \frac{1}{s^2} a_u \right) \qquad \text{Eq. 3.14}$$

Solving equation 3.14 for the disturbance displacement yields

$$w = F_t \left(Z_u \right)^{-1} + \frac{1}{s^2} a_u \qquad \text{Eq. 3.15}$$

The equation for the road disturbance input velocity is derived as follows:

$$F_t = \left(b_u s + k_u \right) \left(w - \frac{1}{s^2} a_u \right) = w \left(b_u s + k_u \right) - \frac{1}{s^2} a_u \left(b_u s + k_u \right)$$

$$w \left(b_u s \right) = F_t + \frac{1}{s^2} a_u \left(b_u s + k_u \right) - k_u w$$

$$ws = \frac{1}{b_u} \left(F_t + \frac{1}{s^2} a_u Z_u - k_u w \right) \qquad \text{Eq. 3.16}$$

Figure 3-4 is the Simulink block diagram representing the open loop estimator. The three inputs are the sprung and unsprung mass accelerations and the control force, which is set to zero. The disturbance displacement and velocity together with the disturbance and tire forces are estimated.

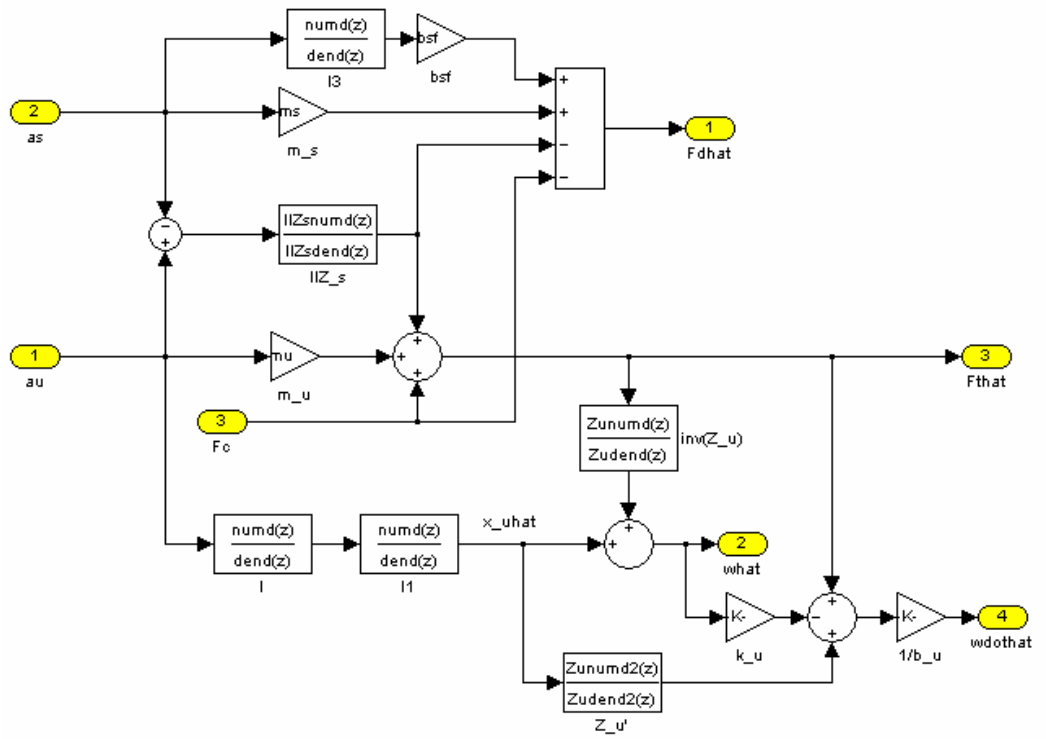

Figure 3-4 Simulink diagram of open loop estimator

The integrators are represented by the I, I1, and I3 blocks. Two integrators are convolved with the suspension impedance equation to create the IIZ_s block. The tire impedance equation is inverted in the inv(Z_u) block. The Z_u' block is the tire impedance convolved with two poles to make the transfer function proper. These pole frequencies are two orders of magnitude higher than the zero frequency so as to not affect the dynamics of the frequency range considered.

4 SIMULATION AND RESULTS

This section begins with a description of the tire coupled quarter-car suspension test rig that was used in this study. Also included is a discussion of the simulations performed in continuous and discrete time and the interpretation of the results. Concluding this chapter is a parameter sensitivity study performed to examine the numerical robustness of the estimator.

4.1 Description of experimental test rig

The tire coupled quarter-car suspension test rig at PERL shown in Figure 4-1 was designed with the capacity to have several different types of suspension mounted to it. The sprung mass of the vehicle is represented by an aluminum plate which has provisions for adding mass. Attached to this plate is any one of the specific suspension mounting plates with brackets. The suspension investigated in this study was the left front corner of a Porsche 911 (996) racecar (Grand Am GS class) which is a MacPherson strut type and very common to other passenger cars. The test rig has provisions for attaching linear motors to the sprung mass to create the disturbance force F_d. For a complete description of the development and design of the test rig, the reader is encouraged to see [9].

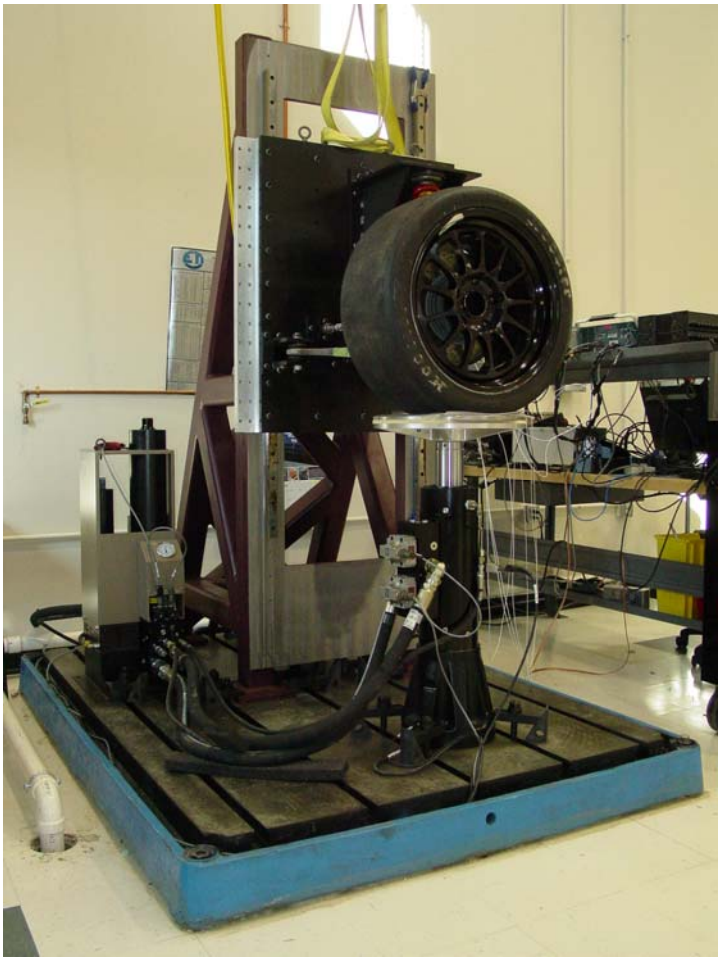

Figure 4-1 Virginia Tech PERL tire coupled quarter-car suspension test rig

A force sensing wheel pan was designed and implemented on the test rig which provides a measurement of the dynamic tire normal force. The wheel pan has three ring type force transducers each with a maximum dynamic load rating of 5000 lb. The sensors are AC coupled devices and consequently unable to measure static forces. During use, an increase in force from a static value corresponds to a positive voltage while a decrease in force corresponds to a negative voltage. These sensors were chosen for their ability to withstand the shear force induced by the tire scrub and/or bump steer and also to accommodate a wide range of simulated vehicles. The pre-load procedure for these transducers was to attach the output of each conditioned signal from the sensor to an oscilloscope and monitor the signal as torque was applied to the fastener. The clamping force created by the fastener was needed to preload the sensors to 1000 lb which corresponded to 1 V. The sensors have a relatively long time constant so the absolute

value of the signal will be seen for a sufficiently long enough time to pre-load the sensors [10]. These sensors and their locations can be seen in Figure 4-2.

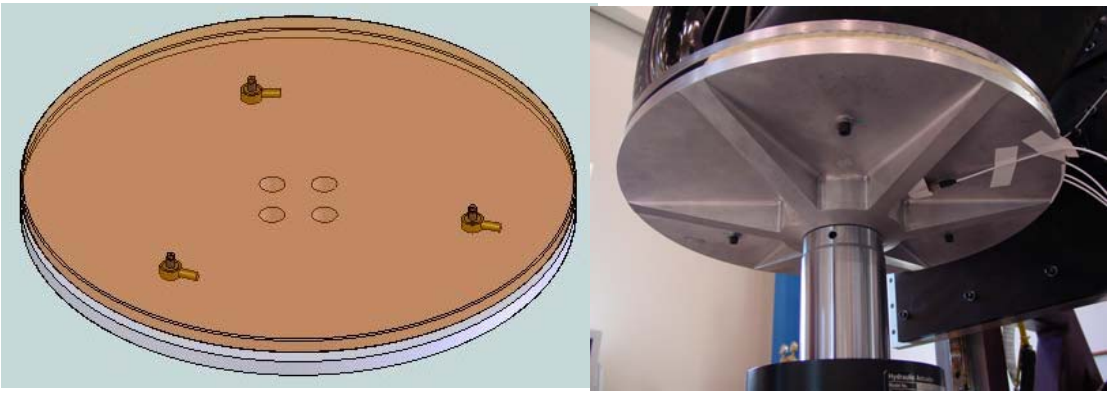

Figure 4-2 Force sensing wheel pan

4.2 Integration methods

Three types of integrators were explored in this study. Beginning the simulations with an ideal integrator was the logical choice since there are few possibilities to cause instabilities. The two other types of integrators can be classified as pseudo integrators, in that they deviate from the standard transfer function of *1/s*. A single real pole low pass integrator was first implemented. This type proved unsatisfactory due to the lack of control over the phase distortion, so a third type of integrator was developed.

This third type was a pair of complex poles with a differentiator. Its behavior was like that of a differentiator below and an integrator above a specified frequency. This behavior was necessary to mitigate a low frequency drifting or instability problem common to double integration of noisy signals, specifically the acceleration signals. The break frequency and damping ratio were tuned to improve stability without too much magnitude and phase distortion of the signals at low frequencies. Figure 4-3 plots the magnitude and phase angle of the three transfer functions for the integrators. The break frequency is 0.5 Hz and the damping ratio is 0.75.

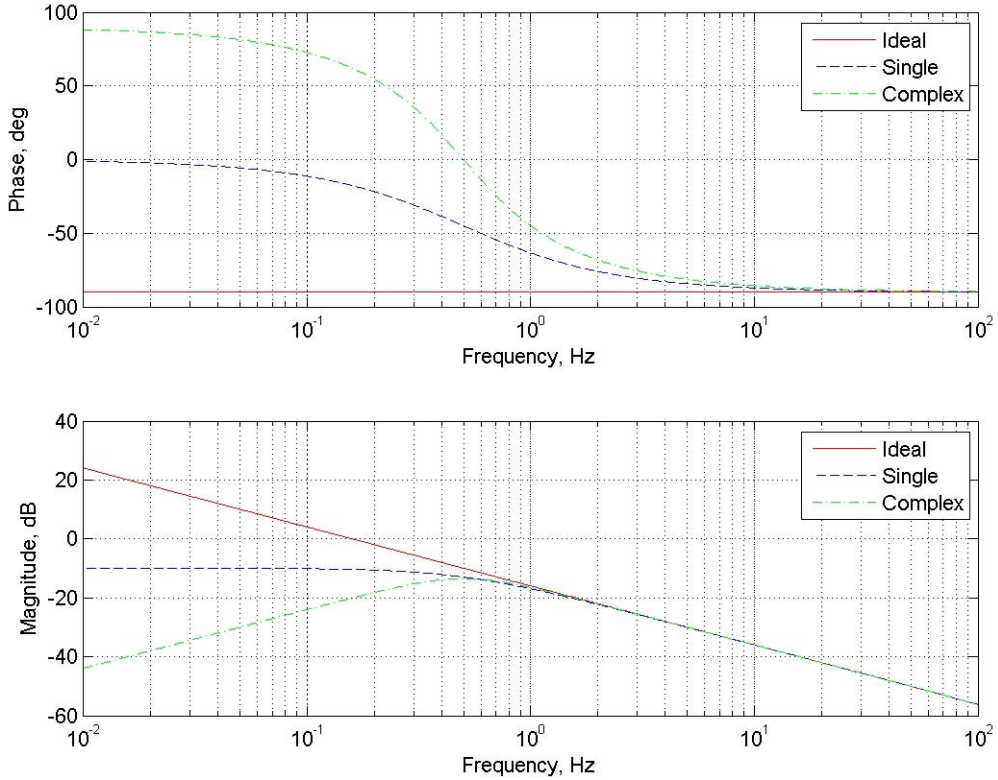

Figure 4-3 Magnitude and phase plot of ideal, single pole and double pole integrators

The transfer functions are given in Table 4-1 where a is the break frequency in rad/s, ζ is the damping ratio, and s is the Laplace operator.

Table 4-1 Transfer functions of various integrators

Ideal	Single Pole	Complex Pole
$\frac{1}{s}$	$\frac{1}{s+a}$	$\frac{s}{s^2+2\zeta a+a^2}$

Regarding the primary and secondary ride frequencies of 5 Hz and 28 Hz, a relatively high break frequency and damping ratio was necessary to decrease the drifting problem when implemented in real-time; therefore the phase is distorted at lower frequencies. This is an inevitable compromise between stable estimates and phase distortion of the estimates at low frequencies.

4.3 Discretization

The continuous time elements in Simulink were converted to discrete time versions by using the bilinear Tustin transform. Allowing dSpace to convert the continuous time blocks to a discrete representation was not acceptable. The Tustin transform from the *s* domain to the *z* domain is

$$s = \frac{2}{t_s}\left(\frac{z-1}{z+1}\right) \qquad \text{Eq. 4.1}$$

where t_s is the sample period. The Tustin transform creates a more accurate discritized version of a continuous time signal relative to a zero order hold (signal assumed constant during sampling interval) or a first order hold (signal assumed piecewise linear during sampling interval).

4.4 Simulation experiments in discrete time

The quarter-car model and estimator parameters used in this section of the study are given in Table 4-2. For an explanation of how these were determined refer to section 5.1.

Table 4-2 Model and estimator parameters used in simulation and experiments

Parameter	Value
m_s	250 kg
b_s	5220 N s/m
k_s	286716 N/m
m_u	34 kg
k_u	423645 N/m
b_u	726 N s/m
b_{sf}	3173 N s/m

After performing the following tests in continuous time, the same tests were completed in discrete time, the results of which are presented in this section. Each set of tests is comprised of three tests; one run with each of the integrators. The first set of tests investigates the influence each of the various integrators has on the estimates by allowing only a wheel pan disturbance displacement as the input. The second set of tests differs

from the first only by changing the input to be a random disturbance force applied to the sprung mass. The third set of tests has both disturbances input simultaneously.

Table 4-3 Description of tests completed in simulation

Test	Input to model
Test 1	Only disturbance displacement
Test 2	Only disturbance force
Test 3	Both disturbance displacement and force

The random disturbance displacement input to the wheel pan was a band limited white noise signal. The signal was passed through a six pole band pass Butterworth filter to limit the frequency range to excite the modes of the model. The frequencies were concentrated toward the sprung mass mode to avoid nonlinear wheel hop events. The disturbance force was also a white noise signal. It was passed through a convolved four pole low pass Butterworth filter to limit the frequency range to that of handling forces on the sprung mass and low frequency aerodynamic forces. The state space quarter-car model acceleration outputs were inputs to the estimator for all tests.

4.4.1 Random disturbance displacement test

This set of tests investigated the estimator when only a wheel pan disturbance displacement was input. Each of the three integration methods was tested. The frequency and damping ratio was 0.1 Hz and 0.3 respectively. The disturbance force applied to the sprung mass was zero for this series of tests. The estimates in the following figures can be distinguished by the “hat” at the end of the label.

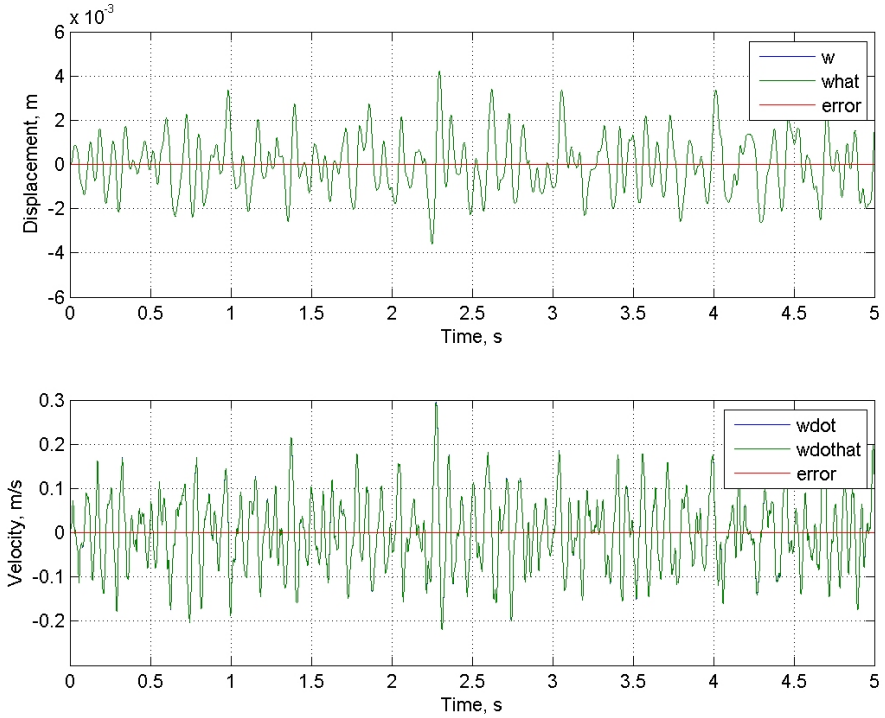

Figure 4-4 Test 1, actual and estimated disturbance displacement and velocity using ideal integrator

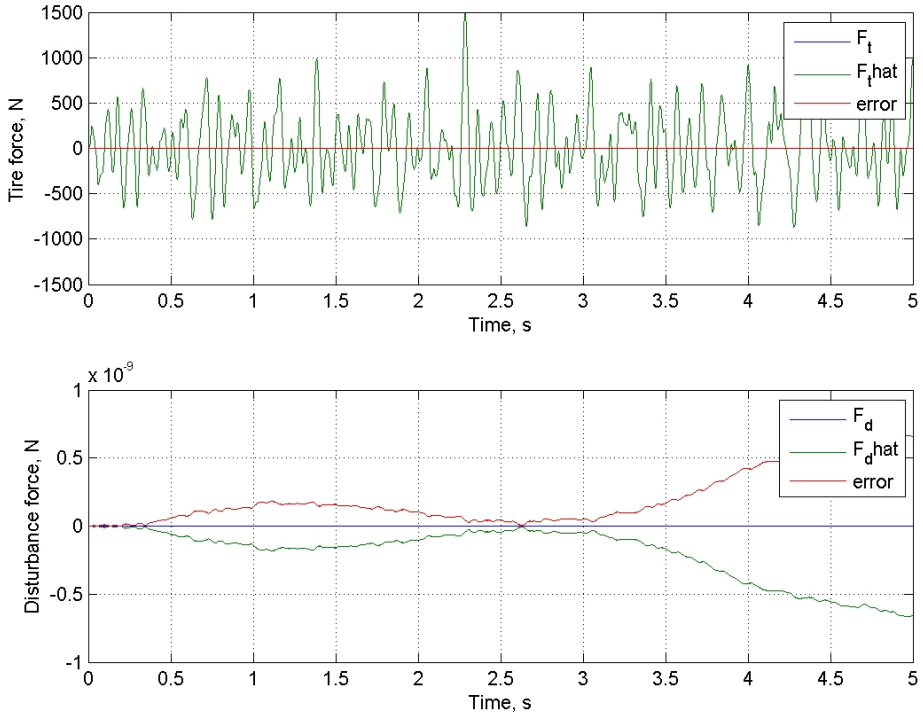

Figure 4-5 Test 1, actual and estimated disturbance and tire force using ideal integrator

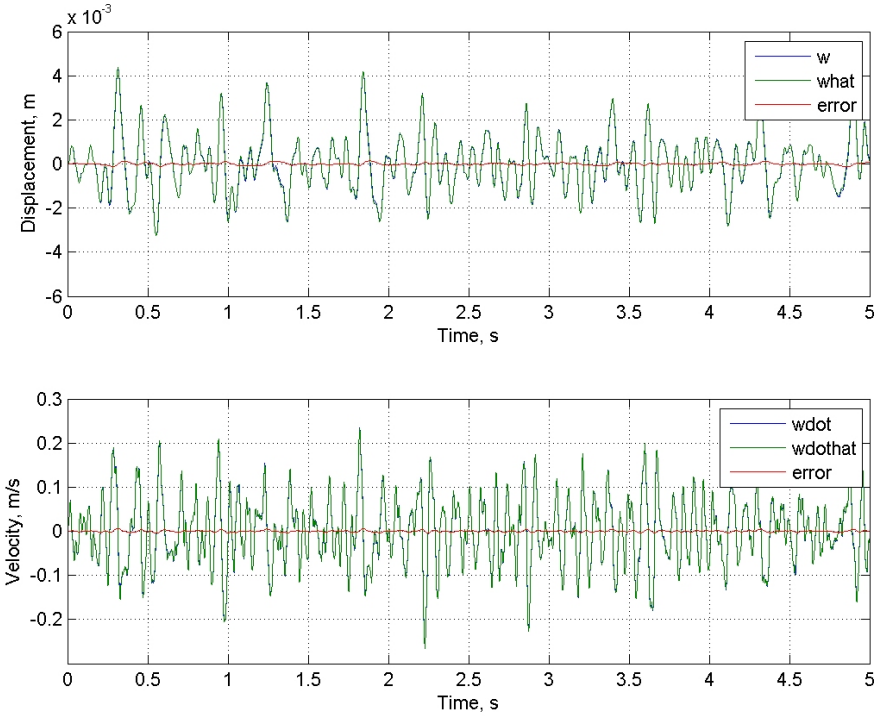

Figure 4-6 Test 1, actual and estimated disturbance displacement and velocity using single real pole integrator

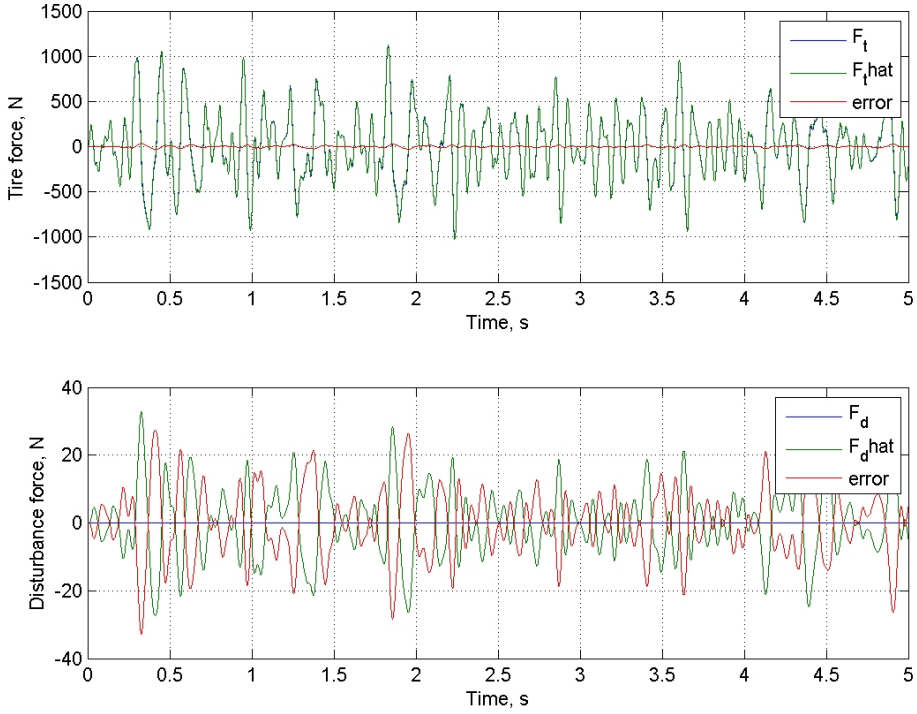

Figure 4-7 Test 1, actual and estimated disturbance and tire force using single real pole integrator

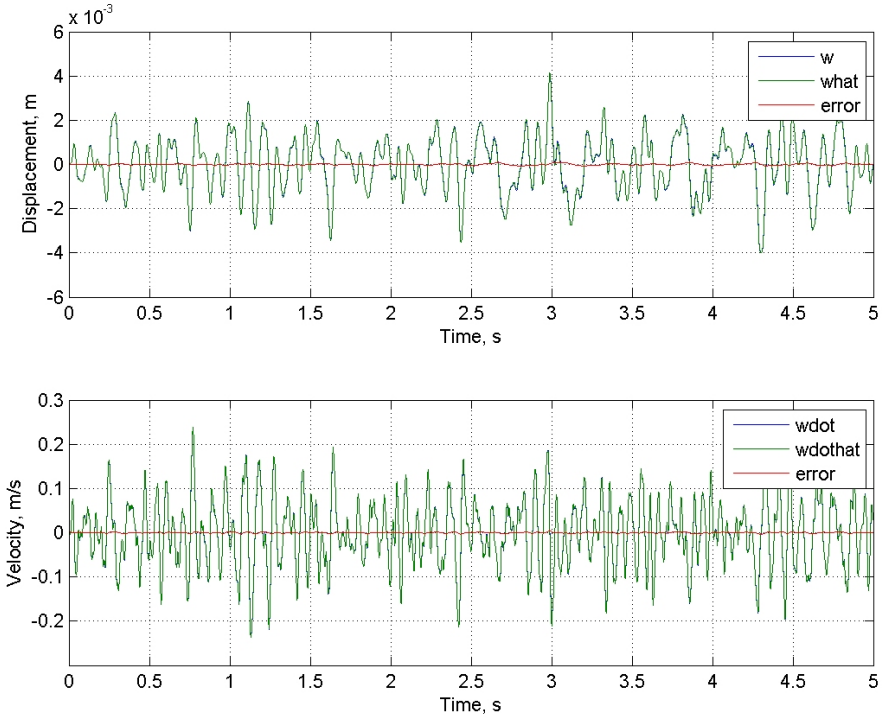

Figure 4-8 Test 1, actual and estimated disturbance displacement and velocity using complex pole integrator

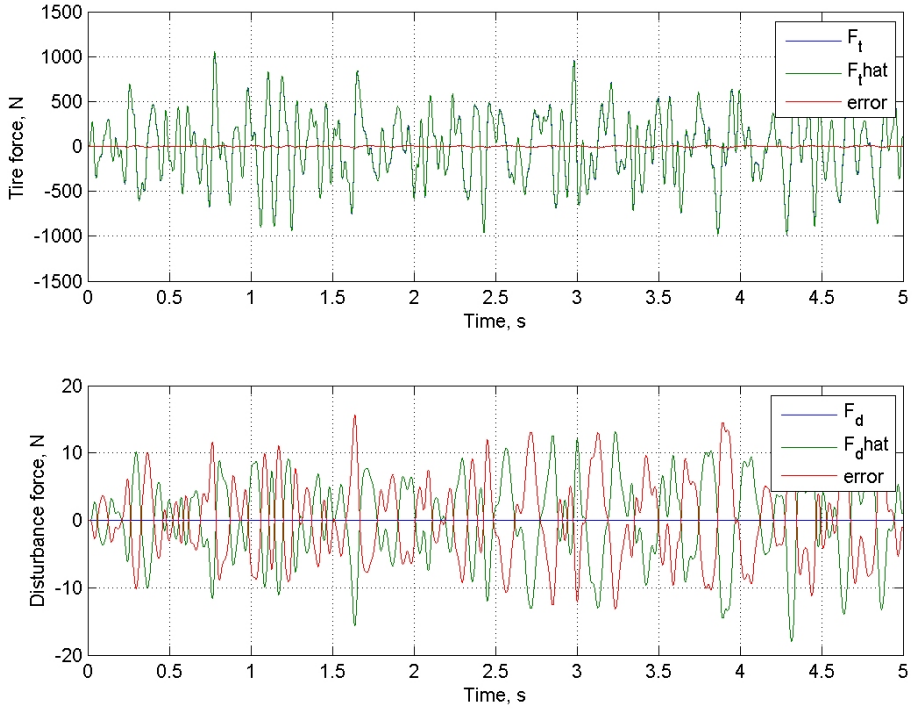

Figure 4-9 Test 1, actual and estimated disturbance and tire force using complex pole integrator

Note the decrease in disturbance force estimation error between Figure 4-7 and Figure 4-9, the real pole and complex pole integrators. The relative insignificance of this error can be put into perspective by noticing the value of the dynamic tire force is two orders of magnitude larger.

4.4.2 Random disturbance force test

This set of tests investigated the estimator when only a disturbance force was input to the sprung mass and the wheel pan displacement was zero. Each of the three integration methods was tested. The frequency of the single real pole was 0.05 Hz. The frequency and damping ratio of the complex pole was 0.03 Hz and 0.3 respectively. The estimation error for the single real pole and complex pole integration methods of the disturbance displacement and velocity is more stable than the ideal integrator but the magnitudes are essentially zero, therefore these figures are omitted.

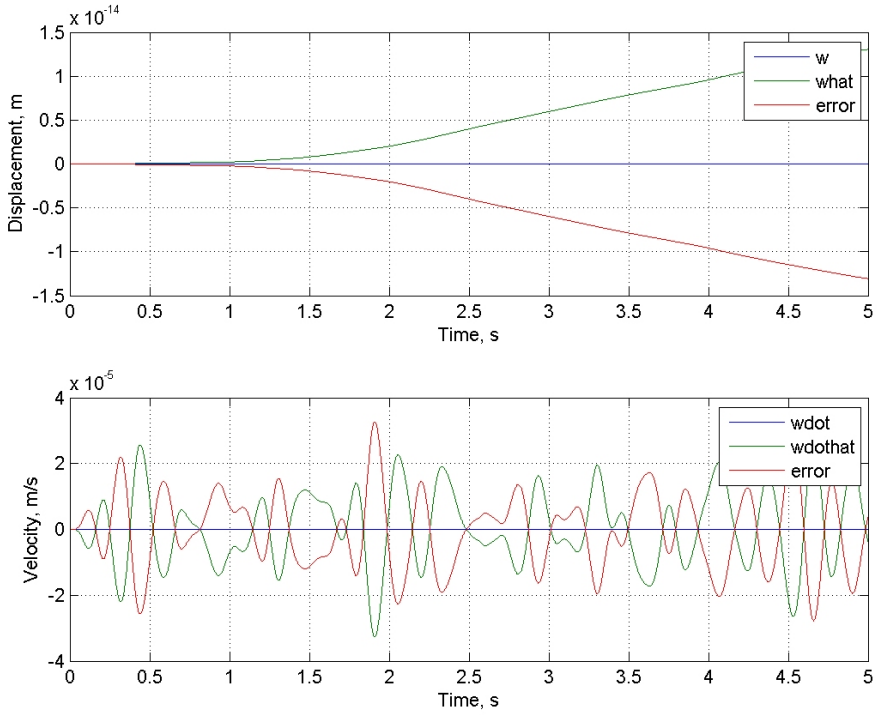

Figure 4-10 Test 2, actual and estimated disturbance displacement and velocity using ideal integrator

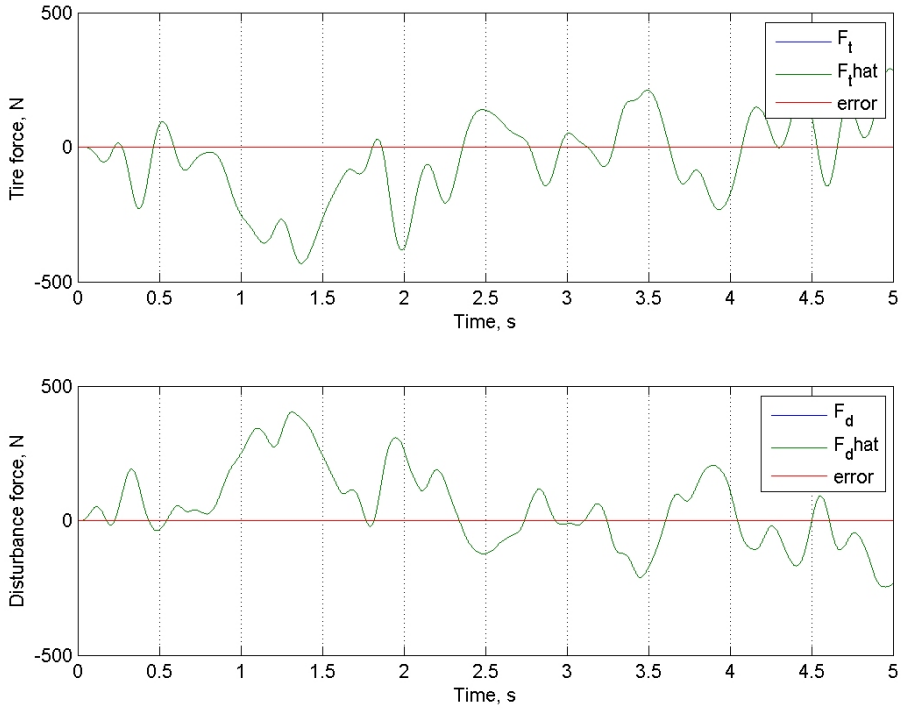

Figure 4-11 Test 2, actual and estimated disturbance and tire force using ideal integrator

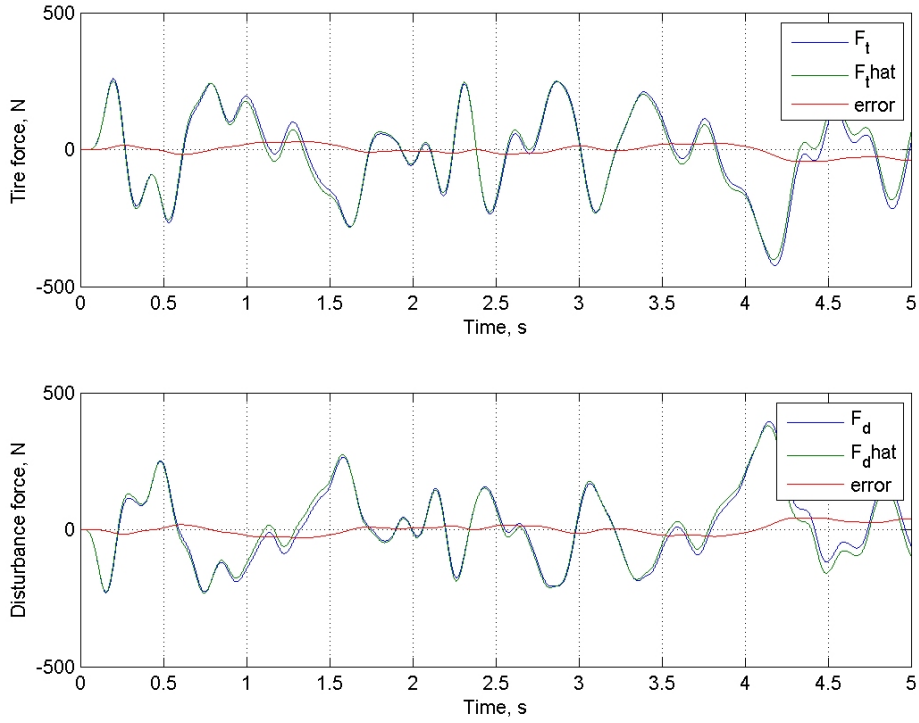

Figure 4-12 Test 2, actual and estimated disturbance and tire force using single real pole integrator

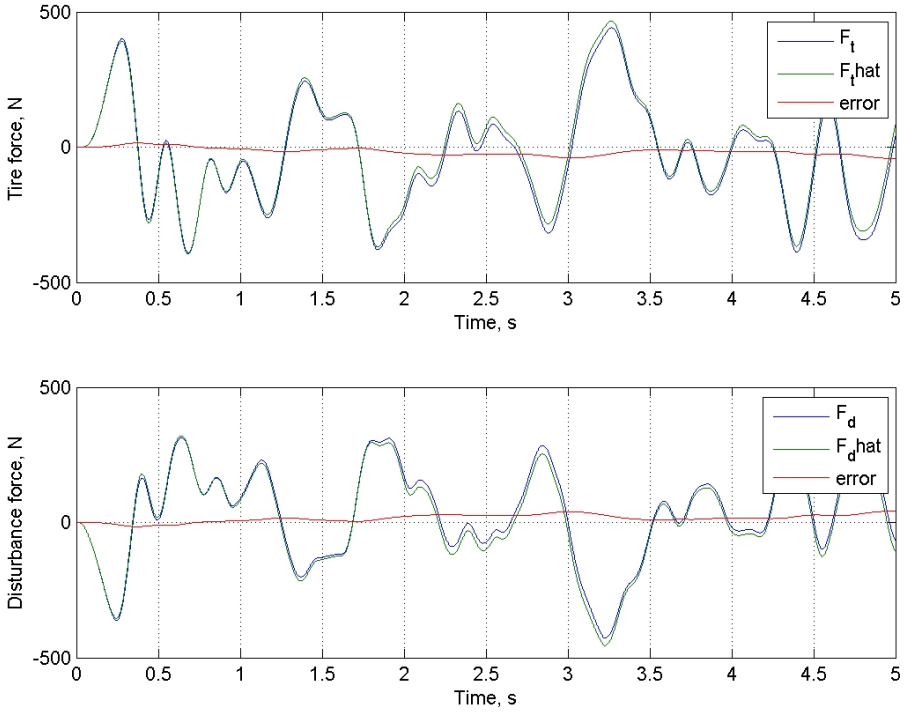

Figure 4-13 Test 2, actual and estimated disturbance and tire force using complex pole integrator

4.4.3 Random disturbance force and displacement test

This set of tests investigated the estimator with a simultaneous wheel pan disturbance input and sprung mass disturbance force input. Each of the three integration methods was tested. The frequency was 0.02 Hz for both the single real pole and the complex pole. The damping ratio of the complex pole was 0.3.

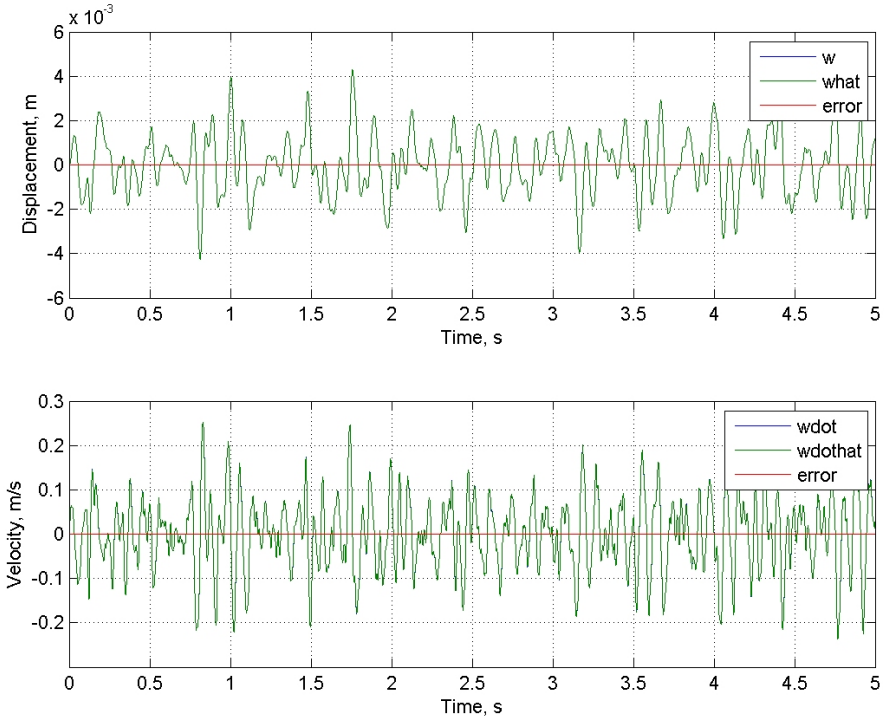

Figure 4-14 Test 3, actual and estimated disturbance displacement and velocity using ideal integrator

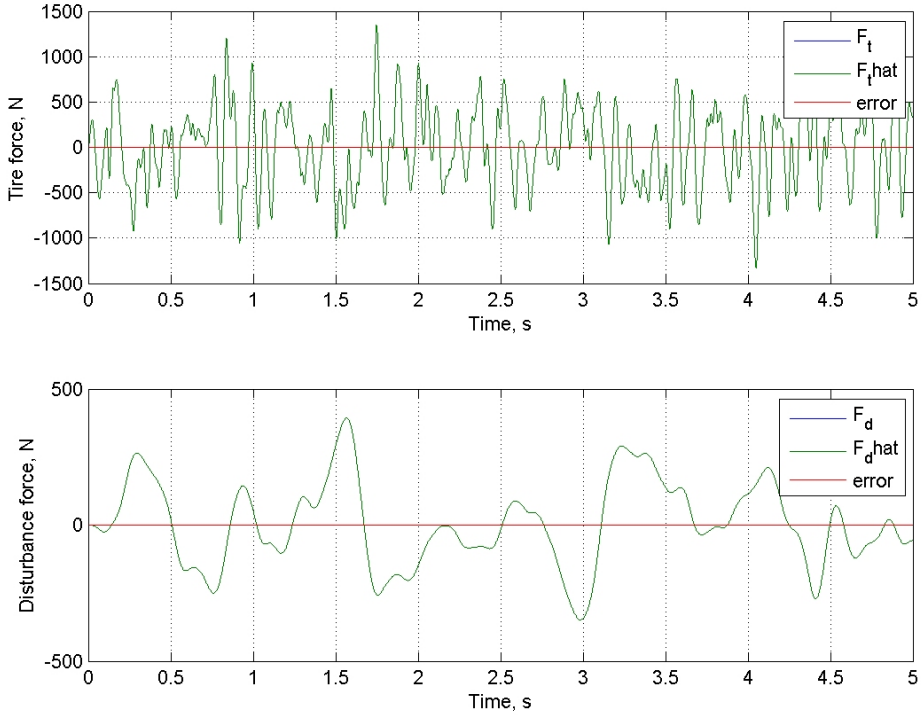

Figure 4-15 Test 3, actual and estimated disturbance and tire force using ideal integrator

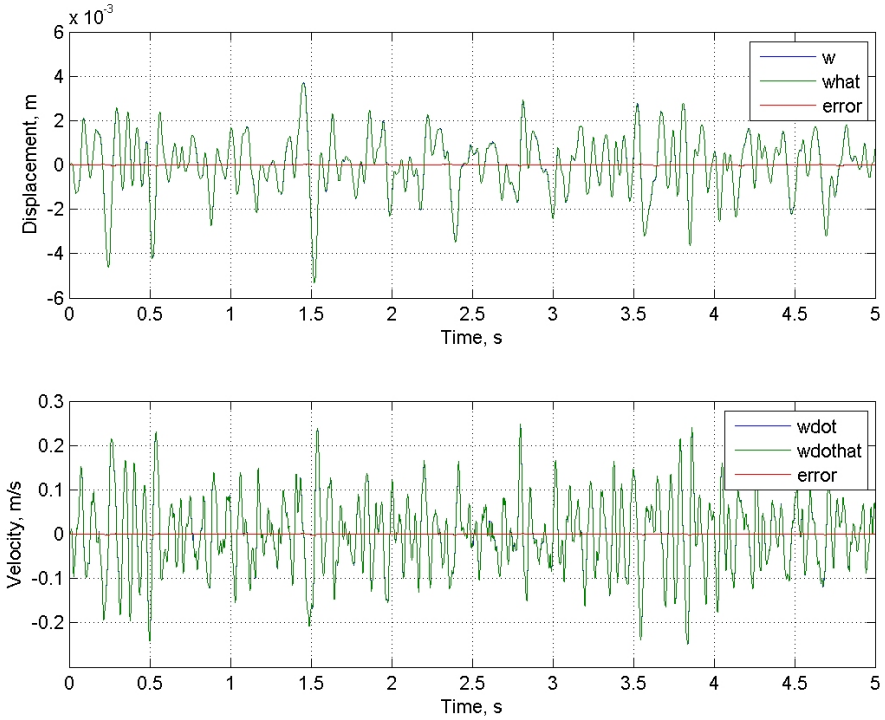

Figure 4-16 Test 3, actual and estimated disturbance displacement and velocity using single real pole integrator

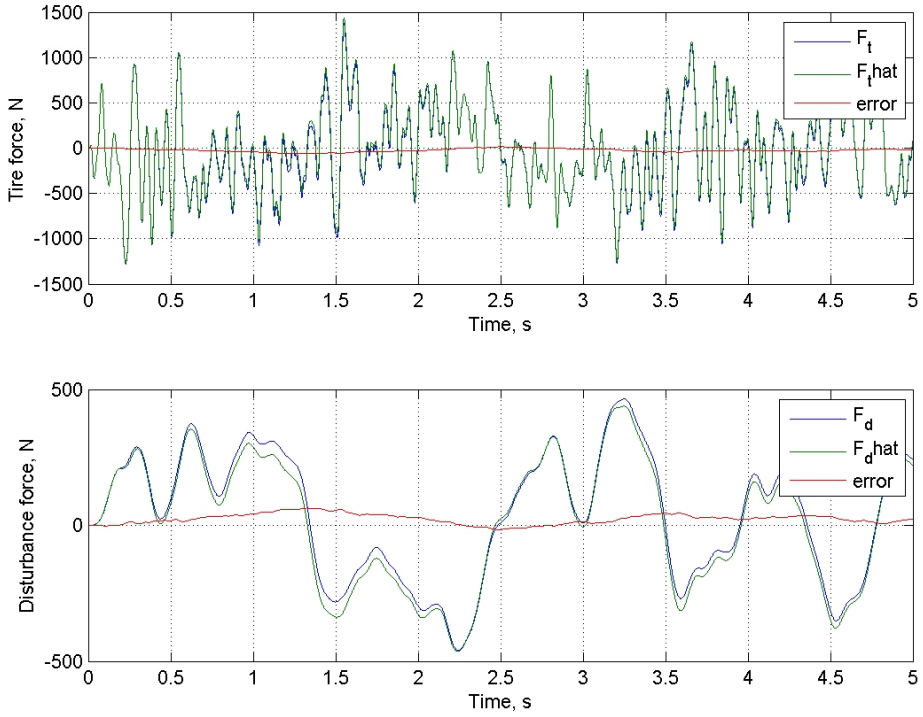

Figure 4-17 Test 3, actual and estimated disturbance and tire force using single real pole integrator

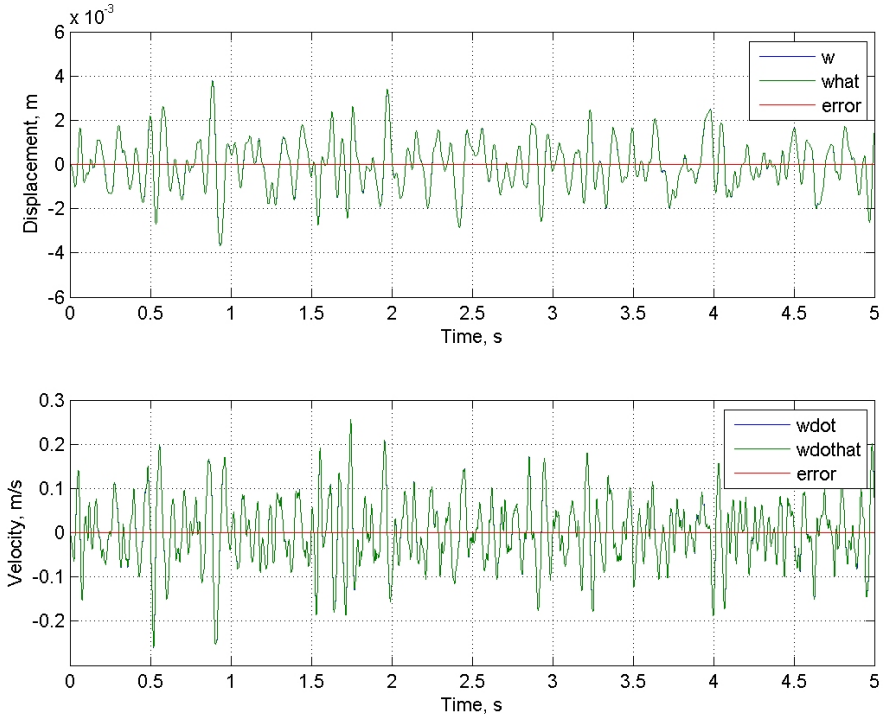

Figure 4-18 Test 3, actual and estimated disturbance displacement and velocity using complex pole integrator

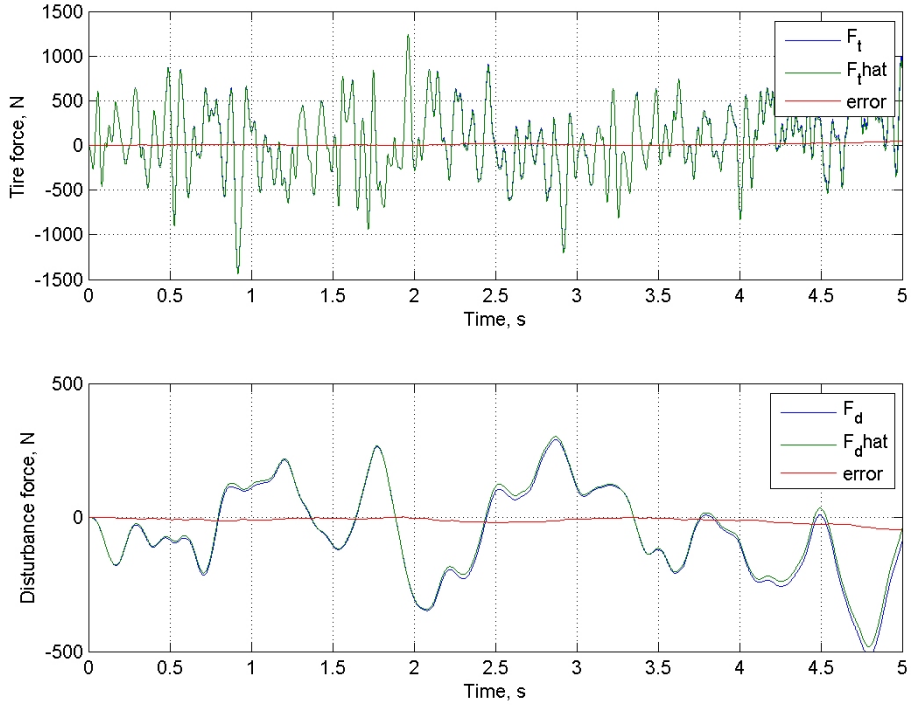

Figure 4-19 Test 3, actual and estimated disturbance and tire force using complex pole integrator

Note the decrease in the force estimation error between Figure 4-17 and Figure 4-19, i.e. the real pole and complex pole integration methods.

4.5 Parameter sensitivity study

A parameter sensitivity study was performed to gauge the robustness of the estimator. Each parameter in the estimator was decreased by twenty percent one at a time while holding all other parameters at their original values. A test was run with the disturbance displacement input only, then a test with the disturbance force input only. Both tests used the ideal integrator. Varying the parameters indicated which values were required to be known with the greatest accuracy in order to obtain decent results from the estimator. A physical meaning for a variation of a parameter is the addition of payload or passengers to the vehicle. A visual inspection of the error between the simulated and estimated signals in order to gauge the effect of varying each parameter was favored over a numerical performance metric, hence the terms "good," "negligible," "small," and "significant". The results are presented in Table 4-4.

Table 4-4 Parameter sensitivity study on estimator parameters

Varied parameter	Random disturbance displacement input	Random disturbance force input	Disturbance displacement and force
m_s	Significant F_d error; w, wdot, and F_t are good	Negligible F_d error; w, wdot, and F_t are good	Significant F_d error; w, wdot, and F_t are good
k_s	Small w, wdot, and F_t error; less significant F_d	Small F_t and F_d error; negligible w error, wdot is	Small w, wdot, and F_t error; significant F_d error
b_s	Small w, wdot, and F_t error; less significant F_d	Negligible F_d error; w, wdot, and F_t are good	Small w, wdot, and F_t error; significant F_d error
b_{sf}	Negligible F_d error; w, wdot, and F_t are good;	Negligible F_d error; w, wdot, and F_t are good	Small F_d error; w, wdot, and F_t are good
m_u	Negligible w, wdot, and F_t error; F_d is good	All estimates are good	All estimates have negligible error
k_u	Significant w and wdot error; F_t and F_d are good	Negligible w error; wdot, F_d, and F_t are good	Small w and wdot error; F_t and F_d are good
b_u	Negligible w and wdot error; F_t and F_d are good	All estimates are good	All estimates are good

The results of this parameter sensitivity study indicated the tire damping was not very sensitive. The parameters associated with the unsprung mass overall were not too sensitive with the exception of k_u during the displacement test. The most sensitive parameters were associated primary suspension and the sprung mass.

4.6 Results of simulation studies

The study of the integration methods indicated the observer is able to provide good estimates of the wheel pan disturbance displacement and velocity as well as the disturbance force and dynamic tire force regardless of the method used. However, the ideal integrator is impractical for real-time implementation since there is no attenuation of magnitude for very low frequencies (near zero). The complex pole integrator was chosen because it provides a high-pass characteristic to control the DC drift associated with real-time integration.

The parameter sensitivity study suggested which quarter-car model parameters were required to be known with the largest accuracy in order for the observer to provide good estimates. The study with only the disturbance displacement input was the most valuable for this study since at the time of this writing, no controllable disturbance force sources exist on the test rig.

5 EXPERIMENTAL PROCEDURES AND RESULTS

This chapter begins by explaining the parameter optimization method used to obtain quarter-car model parameters which fit an experimentally measured acceleration response. Batch acceleration data was input to the estimator and tests were run with the complex pole integrator to investigate different high pass filters for use with the acceleration signals. The results of real-time implementation of the estimator are presented. Development of the dSpace code and a virtual instrument in ControlDesk is also discussed.

5.1 Parameter optimization with measured data

Due to the results of the parameter sensitivity study in Section 4.5, parameter optimization was performed to improve the observer accuracy when implemented in the lab. The parameters of the quarter-car model are identical to those in the estimator. Some of the values were known with adequate confidence while the values of others such as the tire damping and linear guide damping could only be guessed. Acceleration data was collected in the lab with the intention of discovering quarter-car model parameters that would match the acceleration history measured in the lab when the model was excited by the same input. Using the Matlab function *fmincon.m* and entering initial guesses along with upper and lower search bounds for the parameters resulted in parameters that were optimized to fit the measured acceleration data.

The function *fmincon.m* calculates the minimum of a constrained nonlinear multivariable function. This function is a gradient based method; therefore it is possible that the results are only local minima [13]. To try to minimize this possibility it is necessary to have good initial values for the parameters and upper and lower search bounds that are within reason.

At each iteration step, *fmincon.m* is used to compute the sprung and unsprung mass acceleration responses of a quarter-car model using the current values of the parameters

to be optimized. The input to the model is the same as that measured in the lab. The difference between the optimized response and the measured response is computed along with an error vector. This error vector is input to a cost function whose scalar value is output. If no termination conditions are met, *fmincon.m* will not stop. Some termination conditions are exceeding the maximum number of iterations, achieving a smaller variation in minimum cost than specified, and achieving a smaller directional derivative of the gradient than specified.

Once the iteration loop has ended, the acceleration response of the quarter-car model is computed using the optimized parameters. The "optimized" response is plotted against the measured responses along with the remaining error in Figure 5-1.

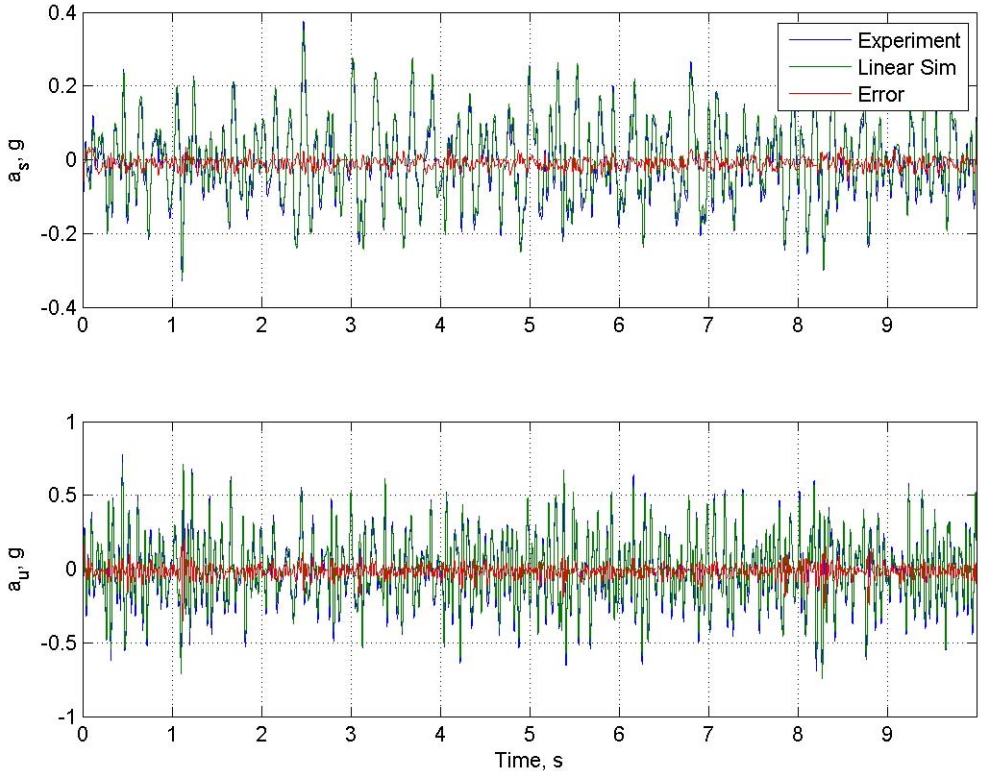

Figure 5-1 Parameter optimization result with experimental and linear model responses

Figure 5-2 is the same as Figure 5-1 but with a magnified time axis. The search bounds for the sprung mass were small since this value was known with the most confidence. The search bounds for the other parameters were twenty percent above and below the

initial values. The frequency content of the disturbance signal input to the wheel pan was of sufficient bandwidth to excite the sprung and unsprung mass modes.

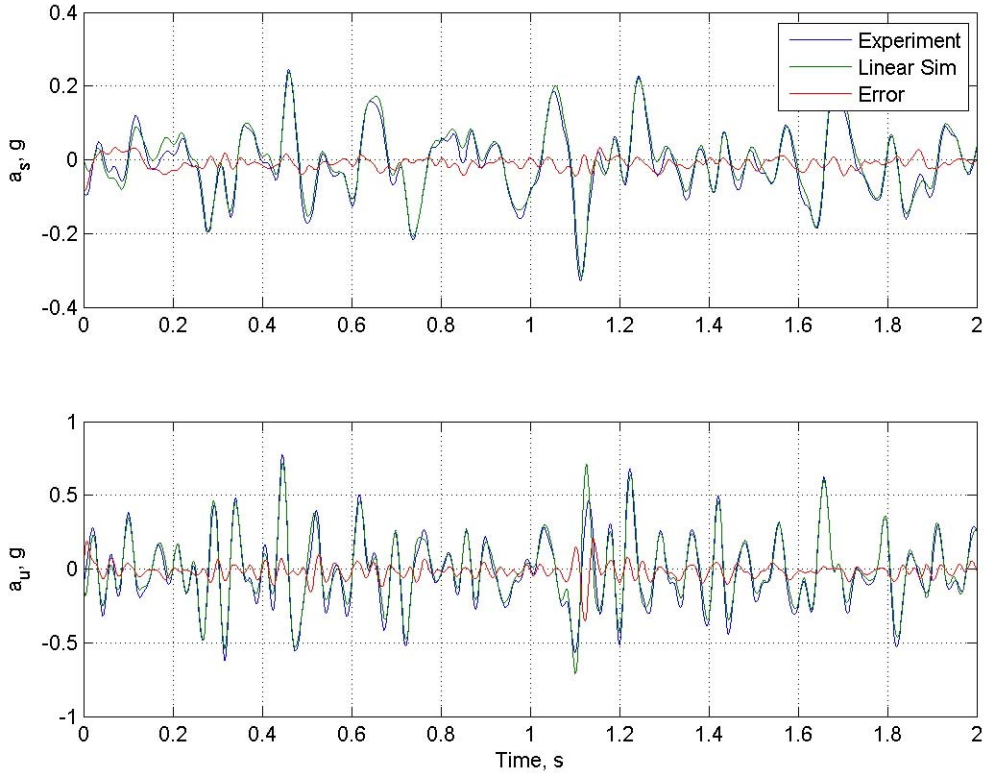

Figure 5-2 P arameter optimization result with experimental and linear model responses (magnified time axis)

These results indicate the linear model adequately predicts the acceleration of the sprung and unsprung mass under this excitation and the resultant optimized parameters should lead to good results from the observer. The initial values for the parameters which were optimized and their optimized values are listed in Table 5-1. It is not necessary for controls design that the optimized values represent the actual components of the test rig. The optimized parameters are intended to elicit the same response from the linear model as the response measured from the test rig.

Table 5-1 Model parameters and optimized model parameters

Parameter	Initial Value	Optimized Value
m_s	246 kg	250 kg
b_s	1400 N s/m	5220 N s/m
k_s	33000 N/m	286716 N/m
m_u	45 kg	34 kg
k_u	385000 N/m	423645 N/m
b_u	100 N s/m	726 N s/m
b_{sf}	10 N s/m	3173 N s/m

5.2 Simulation with measured data

It was discovered through simulations with batch measured acceleration data that in spite of the differentiation behavior of the chosen integration method, the estimator displayed instability at low frequencies. It was decided that the sprung and unsprung mass acceleration signals input to the estimator required additional high pass filtering. Two high pass filters were developed and their transfer functions are given in Table 5-2. Through testing, the filter with the complex pole was favored due to the phase distortion adjustment via the damping ratio.

Table 5-2 Transfer functions of high pass filters for acceleration signals

Single Pole	Complex Pole
$\frac{s}{s+a}$	$\frac{s^2}{s^2+2\zeta a+a^2}$

5.3 Real-time implementation with dSpace

Implementing the estimator in real-time was accomplished via a high speed (1 GHz) real-time rapid control prototyping system, the dSpace AutoBox. It features a sixteen channel analog to digital converter and a six channel digital to analog converter. The channels are simultaneously sampled and have sixteen bit resolution [22]. This system easily interfaces with Matlab and Simulink to implement the developed code in real-time.

Using the virtual instrument software ControlDesk allowed control of various parameters within the Simulink code and the ability to plot desired signals in real-time. The disturbance could be changed from a band limited random signal to a sine signal which could have its frequency varied. The magnitude of the input disturbance could also be varied in real-time. The plotting functions allowed any signal along the Simulink model path to be plotted and viewed.

Since the estimator was constructed with parameters in engineering units such as kg, N/m and N s/m, the acceleration signals input to the estimator were required to have units of m/s^2. Components along the signal path such as the analog to digital converter, signal conditioners, data acquisition system, and the hydraulic system controller all had gains associated with them which needed to be known to ensure proper units on the acceleration signals and the other signals used for comparison.

A multi-rate sampling technique was employed to ensure proper anti-aliasing of the signals input to the analog to digital converter. This was accomplished by the inclusion of a cascaded low pass filter and zero order hold on each signal. This process was applied to all channels to ensure every channel would have the same phase distortion.

5.4 Real time results

The real-time tests began with a sine disturbance input to the test rig since dynamic responses due to a sine input are much easier to diagnose than a random input. The disturbance input to wheel pan was a ±2 mm amplitude sine wave where the frequency was swept from 3 to 19 Hz. Magnitudes and phase angles of various points in the signal path were checked in real-time to ensure the signals entering the estimator were reasonable. Figure 5-3 is the disturbance displacement and velocity estimate to a 3 Hz signal. Notice the errors are due mainly to phase distortion resulting from the integration method and is expected to decrease at higher frequencies. The tire force estimate in Figure 5-4 indicates a better phase angle match between the measured and estimated signals. The magnitude error in the tire force estimate is likely due to the low accelerometer signal strengths at this frequency.

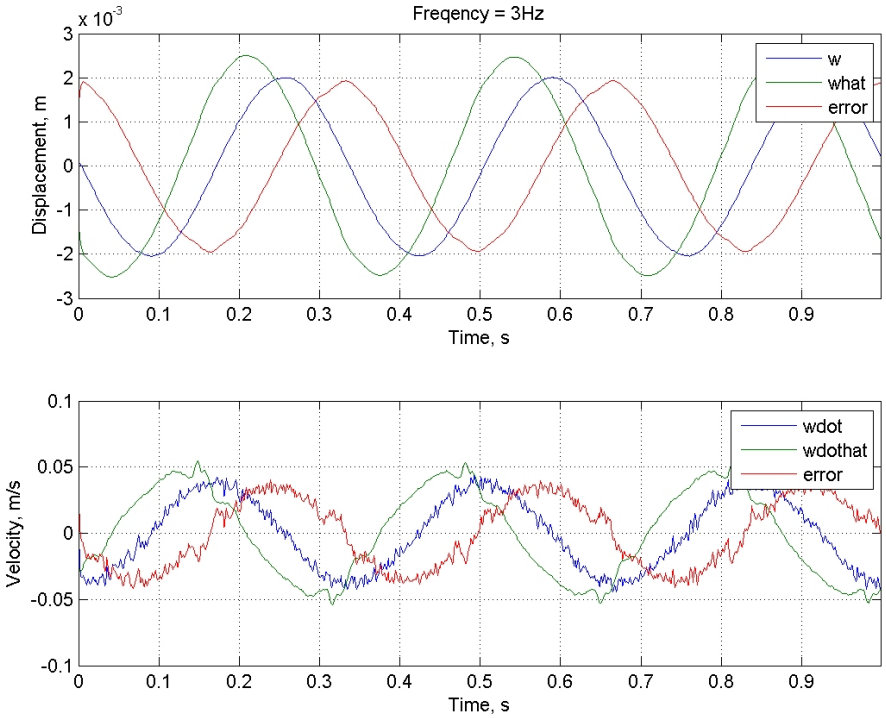

Figure 5-3 Actual and estimated disturbance displacement and velocity for 3 Hz sine input

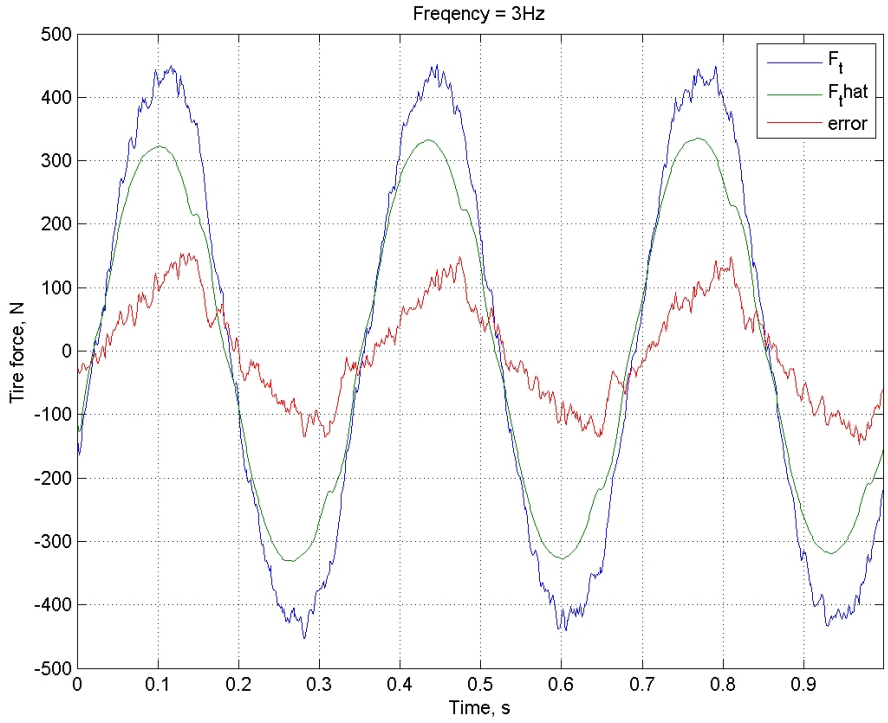

Figure 5-4 Actual and estimated tire force for 3 Hz sine input

The estimates of wheel pan disturbance displacement and velocity for a 5 Hz sine input are shown in Figure 5-5 and the tire force estimate in Figure 5-6. The tire force estimate is quite good, while the phase angle difference is improved for the disturbance displacement and velocity estimates relative to the 3 Hz input.

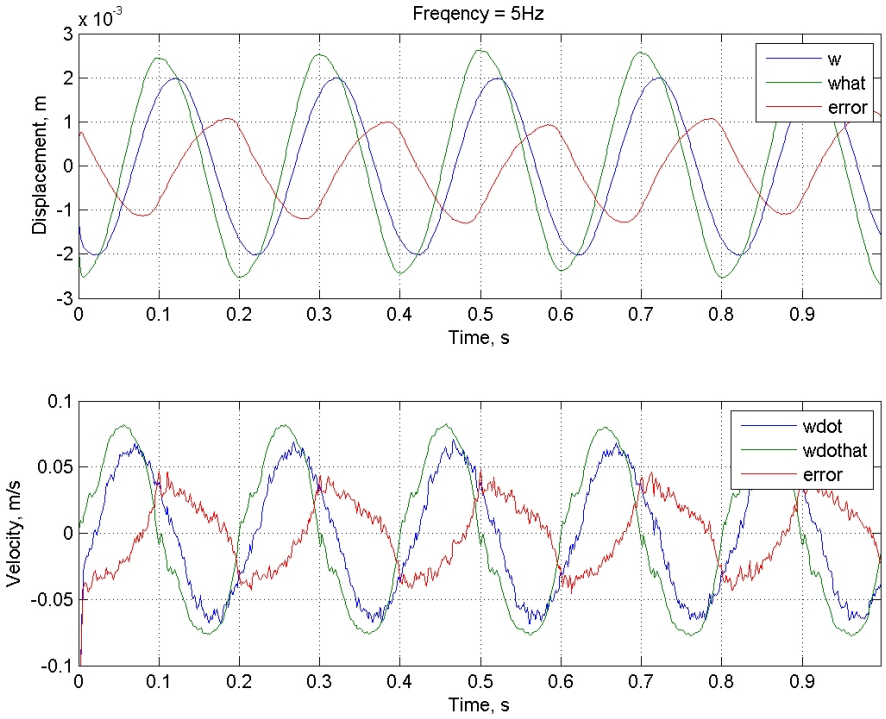

Figure 5-5 Actual and estimated disturbance displacement and velocity for 5 Hz sine input

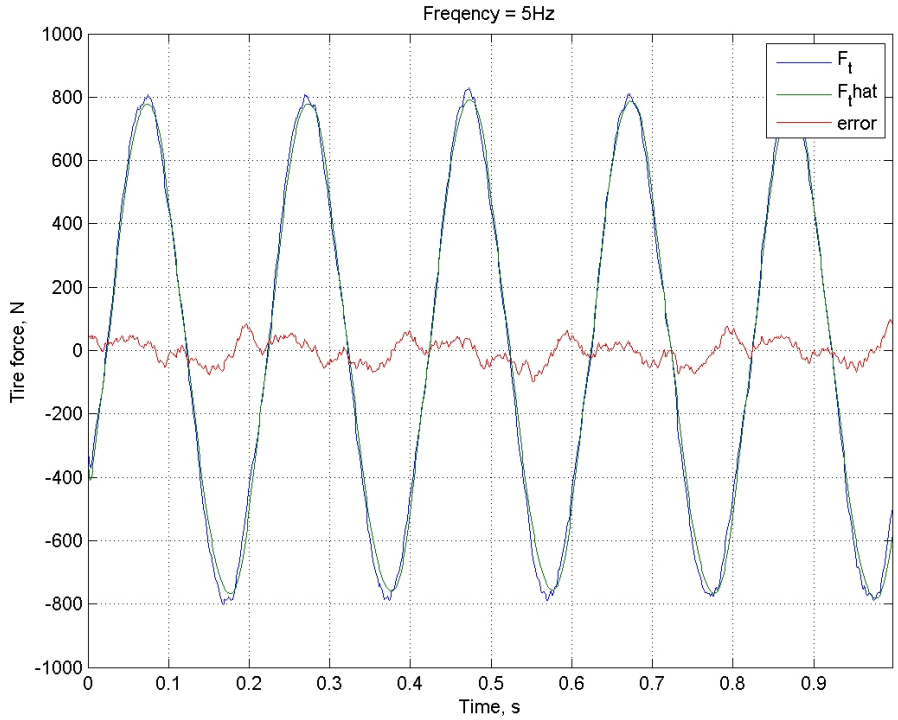

Figure 5-6 Actual and estimated tire force for 5 Hz sine input

The 12 Hz and 17 Hz excitations showed much improved magnitude and phase error in the wheel pan disturbance displacement and velocity estimates. The tire force estimate did not degrade significantly.

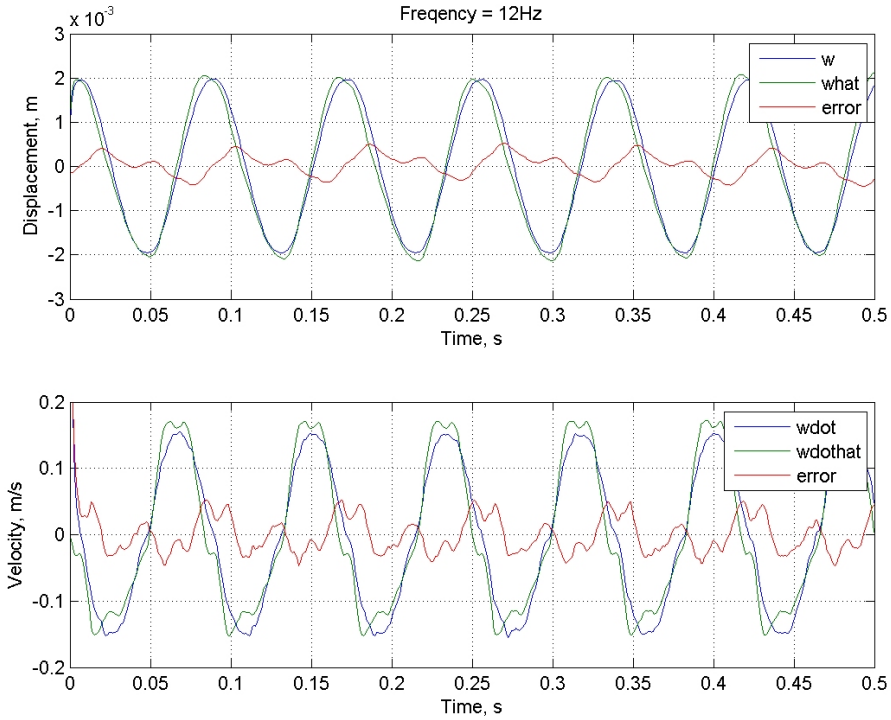

Figure 5-7 Actual and estimated disturbance displacement and velocity for 12 Hz sine input

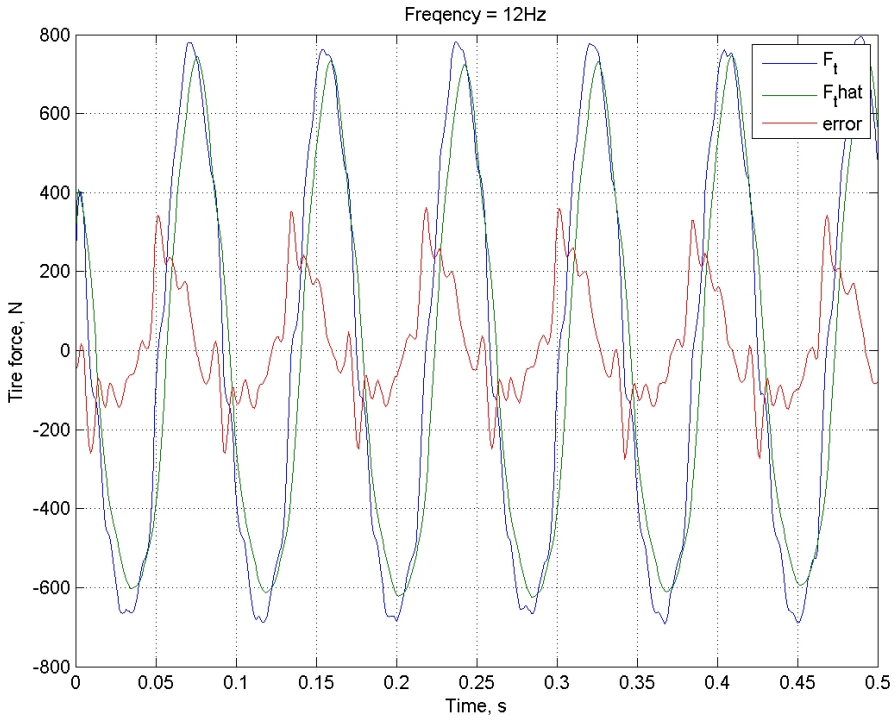

Figure 5-8 Actual and estimated tire force for 12 Hz sine input

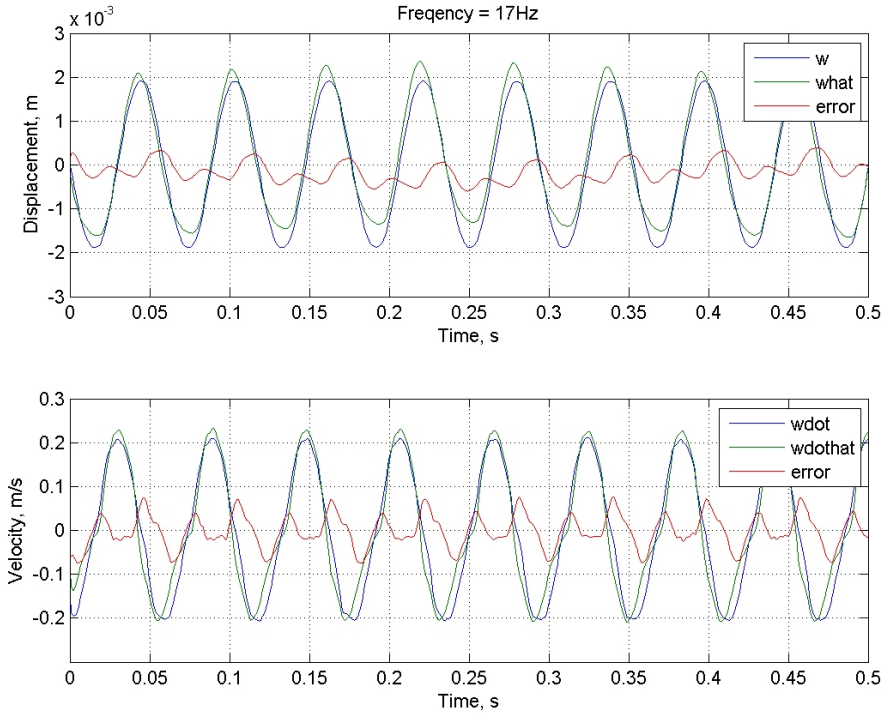

Figure 5-9 Actual and estimated disturbance displacement and velocity for 17 Hz sine input

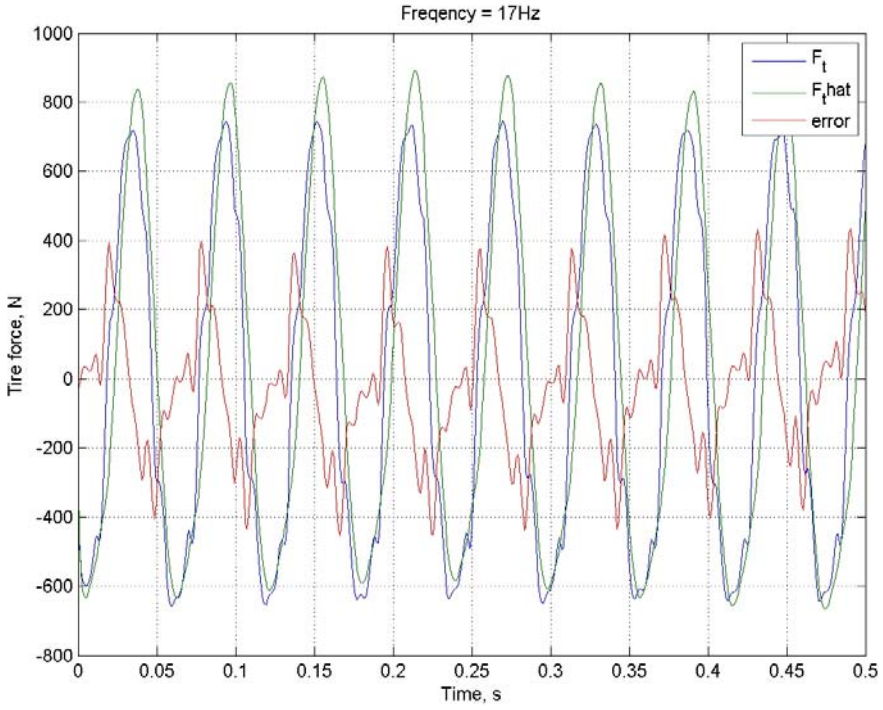

Figure 5-10 Actual and estimated tire force for 17 Hz sine input

Since these sinusoidally excited data sets each have a single excitation frequency, this enabled the creation of a frequency response curve via calculation of the Fourier coefficients of desired signals at each frequency. Performing similar calculations with the response of the linear quarter-car model to the same input would reveal whether the acceleration signals entering the observer and the tire force were yielding reliable results.

The magnitude and phase angle of the dynamic tire force, sprung mass acceleration, and unsprung mass acceleration are plotted on a log scale. The experimental data from the rig is represented by dashed lines in Figure 5-11 and the quarter-car model by solid lines. The phase angle of the acceleration signals is displayed relative to the phase angle of the tire force signal. Notice the magnitudes of the acceleration signals of the quarter-car model are acceptable for use in active control methods applied to vehicle suspensions compared with the actual rig. This indicates that the linear model is an acceptable representation of the actual system for this application. The dynamic tire normal force experimental and simulated magnitude curves are acceptable until near 15 Hz where the similarity degrades. Further testing at higher frequencies that include the secondary ride frequency would be necessary to determine if this is an impending nonlinearity.

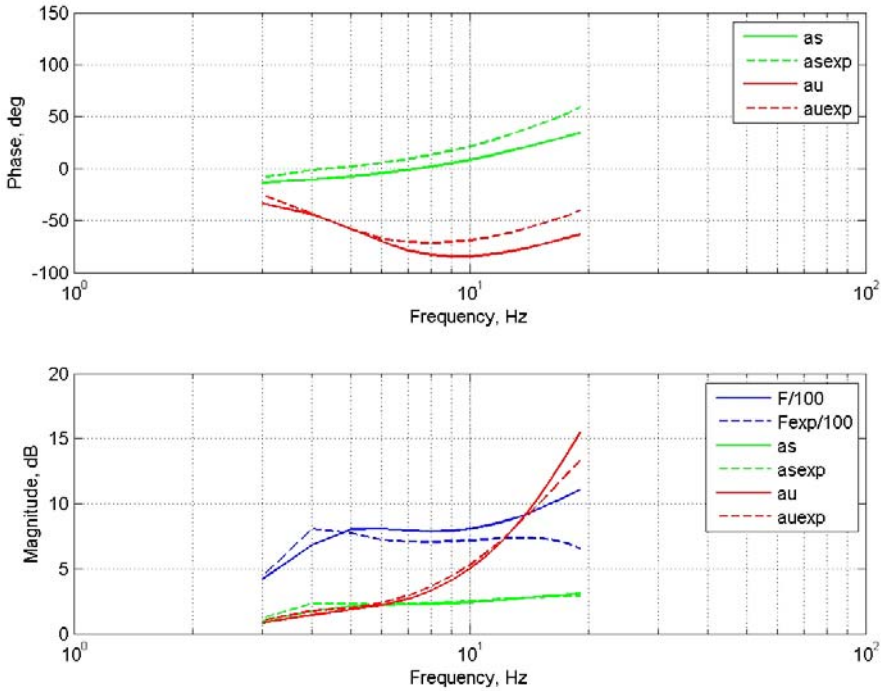

Figure 5-11 Magnitude and phase comparison between simulated and experimental plants

Once the acceleration signals entering the observer were validated, the input was changed to a band limited white noise disturbance. Figure 5-12 shows a section of the data where the observer is providing decent estimates of the disturbance displacement and velocity. Figure 5-13 is the estimated tire force during this same time interval.

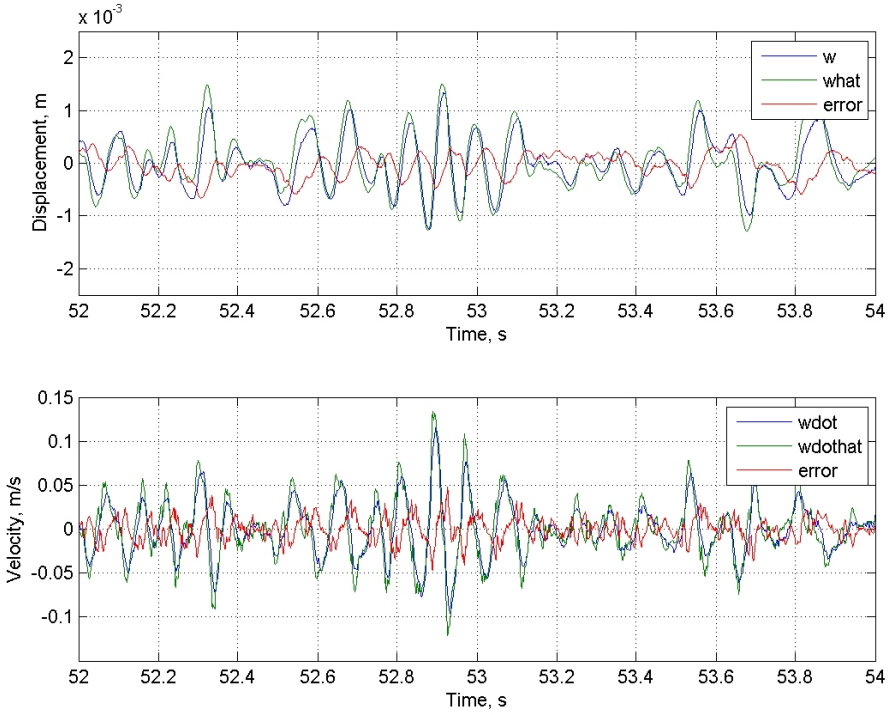

Figure 5-12 Real-time disturbance displacement and velocity response to random input (good)

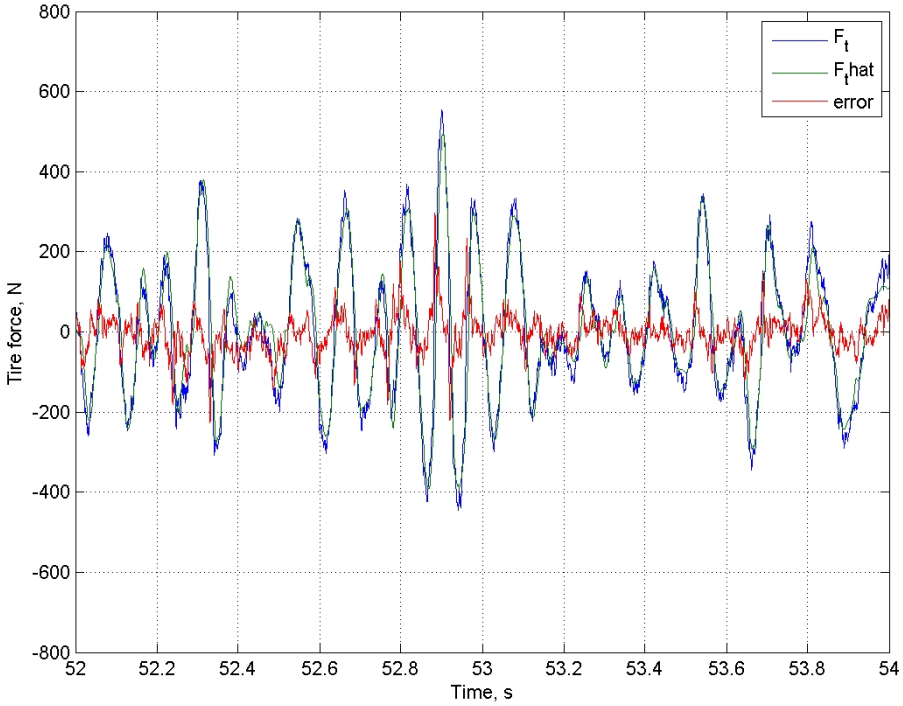

Figure 5-13 Real-time tire force response to random input (good)

An occasional low frequency drift occurred during this test. Figure 5-14 shows this phenomenon in the disturbance displacement estimation error signal. Note the disturbance velocity does not display this drift. Figure 5-15 shows how this drift affected the estimate of the dynamic tire force.

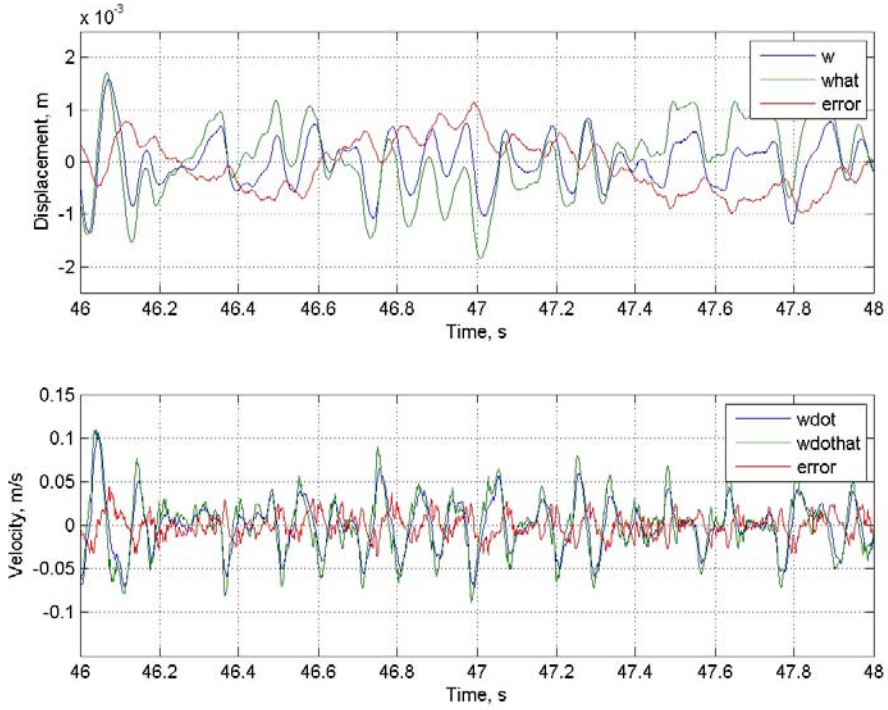

Figure 5-14 Real-time disturbance displacement and velocity response to random input (poor)

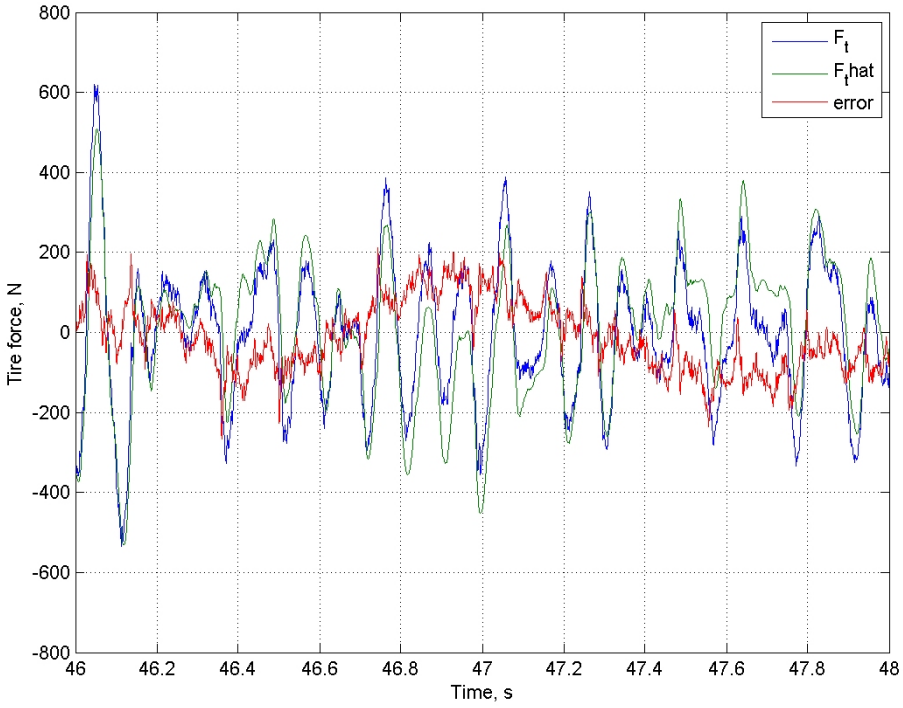

Figure 5-15 Real-time tire force response to random input (poor)

The method used for quantifying the performance of the observer was comparing the root mean squared value of the power contained in the measured signal to the power remaining in the residual error between the measurement and the estimate. Vectors **e** and **p** are the error and measured signals, respectively. These vectors are constructed from a 60 s data measurement at a sample rate of 1000 Hz. The vector **p** represents the measured disturbance displacement, the measured transmitted tire force, or the real-time calculation of the disturbance velocity. The error was calculated as the difference between the measured signal and its corresponding estimate. The calculation of the root mean squared error in dB is

$$10 \log\left(\frac{mean\left(\mathbf{e}\mathbf{e}^T\right)}{mean\left(\mathbf{p}\mathbf{p}^T\right)}\right) \qquad \text{Eq. 5.1}$$

The calculation in percent is

$$\left(\sqrt{\frac{mean\left(\mathbf{e}\mathbf{e}^T\right)}{mean\left(\mathbf{p}\mathbf{p}^T\right)}}\right)\cdot 100 \qquad \text{Eq. 5.2}$$

The results of the error calculations are summarized in Table 5-3. The observer provided a better disturbance velocity estimate than a disturbance displacement estimate. The tire force estimate was better than the disturbance displacement and velocity estimates.

Table 5-3 Results of root mean square error analysis for disturbance and transmitted force estimates

Estimate	RMS Value	RMS %
w	-9.8 dB	61.3 %
wdot	-15.4 dB	46.3 %
F_t	-21.8 dB	33.6 %

6 CONCLUSIONS AND RECOMMENDATIONS

6.1 Conclusions

The overall intent of this study was to develop a proof of concept which was to implement linear methods to estimate the unmeasured disturbance inputs to the quarter-car test rig in real-time. Since the observer equations were constructed assuming the disturbance input to the wheel pan was a velocity rather than a displacement, it follows that the estimate of this state would be better than the disturbance displacement. The results displayed in Table 5-3 confirm this and also show the estimate of the dynamic tire force contained the least amount of error. This latter result is due to the tire force calculation involving the least amount of integrators and optimized parameters.

The low frequency drift phenomenon was not completely eradicated and some of the error in the disturbance estimates can be attributed to this problem. The stability of the estimates for this open loop observer was very dependent on the signal strength entering the observer and the break frequency of the integrators and high pass filters. Increasing the break frequencies resulted in too much phase distortion at the sprung mass natural frequency of around 5 Hz.

6.2 Recommendations for future work

An interesting solution to improving the stability and accuracy of the disturbance estimates is disturbance accommodation control. This is a closed loop method which lends itself to increased tunability. Disturbance accommodating control is also capable of treating modeling errors as disturbances. As a result, this method would be more robust in the aspect of knowing the values for the masses, damping coefficients, and spring coefficients. The observer developed in this study can predict the point of tire lift off if the free length of the tire spring is known. Once lift off occurs, the estimates are no longer valid since tire lift off is a nonlinear phenomenon. Due to the robustness of the

DAC method which can treat nonlinearities as disturbances, it may be possible to construct an observer to better manage tire lift off.

The frequency range of the disturbance input to the wheel pan in this study was limited to excite primarily the sprung mass mode. The magnitude of the frequency content near the unsprung mass mode of 28 Hz was an order of magnitude lower. The intent of this limitation was to avoid nonlinearities occurring at or near the wheel hop frequency. Further testing should be conducted to investigate the plausibility of the estimates when the magnitude of the disturbance input to the wheel pan near this frequency has a larger magnitude.

The value of the linear bearing damping coefficient and dynamic nature of this damping are unknown. Special low viscosity lubricant was used during installation of the test rig; therefore the value of the damping coefficient obtained via the parameter optimization algorithm seems high. The force due to this damping alone was not negligible during the simulation tests. Inclusion of the linear motors and consequently a measurable source of the disturbance force is necessary to validate the results indicated in the simulation section regarding the estimation of the disturbance force.

Through the course of this study it was discovered that the quarter-car test rig behaves similarly to the developed linear quarter-car model under the magnitude and frequency range involved in this study. This result indicates that future studies involving the suspension used in this analysis can begin with linear theories before considering nonlinear algorithms.

REFERENCES

1. Gordon, T. J., Sharp, R. S. "On Improving the Performance of Automotive Semi-active Suspension Systems Through Road Preview." Journal of Sound and Vibration, Vol. 217 pp. 163-182, 1998.

2. Bender, E. K. "Optimal Linear Preview Control with Application to Vehicle Suspension." Journal of Basic Engineering, Transactions of the American Society of Mechanical Engineers, June 1968.

3. Hac, A. "Design of Disturbance Decoupled Observer for Bilinear Systems." Transactions of the American Society of Mechanical Engineers, December 1992.

4. Hedrick, J. K., Rajamani, R., Yi, K. "Observer Design for Electronic Suspension Applications." Vehicle System Dynamics, Vol 23 pp. 413-440, 1994.

5. Yi, Kyongsu, Song, Byung Suk. "Observer Design for Semi-active Suspension Control." Vehicle System Dynamics, Vol 32 pp. 129-148, 1999.

6. Buckley, A. P., Johnson, C. D. "Complexity Mitigation by Active Control." American Institute of Aeronautics and Astronautics, AIAA-98-4514.

7. H. Imine, Y. Delanne, N. K. M'Sirdi. "Road Profile Input Estimation in Vehicle Dynamics Simulation." Vehicle System Dynamics Vol. 44 No. 4 pp 285-303, 2006.

8. Johnson, C. D., Leondes, C. T. (Ed.), C*ontrol and Dynamic Systems*. Vol 12 Ch 7, 1976.

9. Langdon, J. "Design and Adaptive Control of a Lab Based Tire Coupled Quarter-car Suspension Test Rig for the Accurate Re-creation of Vehicle Response." Master's thesis, Virginia Tech, Blacksburg, VA 2007.

10. Model 201B05 ICP® Dynamic Force Sensor Installation and Operation Manual. PCB Piezotronics Depew, NY 2006.

11. Moran, T., Sullivan, M., Menmuir, D., Mahoney, J. "Replication of Heavy Truck Dynamic Wheel Loads Using a Road Simulator." 4th International Symposium on Heavy Vehicle Weights and Dimensions, Ann Arbor, MI, 1995.

12. "Wheel Force Measurement: RoaDyn Measuring Wheels and Measuring Hubs for Every Application." www.kistler.com April 21, 2007.

13. Matlab R2006b help file for fmincon.m, The MathWorks, Inc 2006.

14. Muijderman, J. H. E. A., Kok, J. J., Huisman, R. G. M., Veldpaus, F. E., Van Heck, J. G. A. M. "Preview Based Control of Suspension Systems for Commercial Vehicles." Vehicle System Dynamics Vol. 32 pp 237-247, 1999.

15. Ogata, Katsuhiko. *Discrete-time Control Systems*, 2nd ed. Prentice-Hall, Inc. Englewood Cliffs, NJ. 1995.

16. Franklin, G. F., Powell, D. J., Workman, M. *Digital Control of Dynamic Systems* 3rd ed. Addison Wesley Longman, Inc. Menlo Park, CA. 1998.

17. Kaynak, M. O. "Multi-step Ahead Prediction Based on the Principle of Concatenation." Proceedings of the Institution of Mechanical Engineers Vol 207 1993.

18. Shook, D. S., Mohtadi, C., Shah, S. L. "Identification for Long Range Predictive Control." IEE proceedings-D Vol 138 No 1, 1991.

19. Kambhampati, C., Manson, J. D., Warwick, K. "A Stable One Step Ahead Predictive Control of non Linear Systems." Automatica Vol 36 (2000) pp. 485-495.

20. Levitt, J. A., Zorka, N. G. "The Influence of Tire Damping in Quarter Car Active Suspension Models." Journal of Dynamic Systems, Measurement and Control Division, Transactions of the ASME Vol 113 pp. 134-137, 1991.

21. Hrovat, D. “Survey of Advanced Suspension Developments and Related Optimal Control Applications.” Automatica Vol 33 No 10 pp. 1781-1827, 1997.

22. dSpace modular Systems Manual. “Hardware Installation and Configuration Reference, for release 5.0.” dSpace GmbH, Germany 2005.

23. Saeger, K. M., Ferris, J. B. "Plausibility Checking of Road Profile Measurements," Journal of Passenger Cars: Electronic and Electrical Systems, paper 2003-01-0669, SAE, Detroit, MI. 2003.

APPENDIX

Quarter-car state space matrices

$$\mathbf{A}=\begin{bmatrix} 0 & 1 & 0 & 0 & 0 \\ -\frac{k_s}{m_s} & -\left(\frac{b_s+b_{sf}}{m_s}\right) & \frac{k_s}{m_s} & \frac{b_s}{m_s} & 0 \\ 0 & 0 & 0 & 1 & 0 \\ \frac{k_s}{m_u} & \frac{b_s}{m_u} & -\left(\frac{k_s+k_u}{m_u}\right) & -\left(\frac{b_s+b_u}{m_u}\right) & \frac{k_u}{m_u} \\ 0 & 0 & 0 & 0 & 0 \end{bmatrix} \quad \mathbf{B}=\begin{bmatrix} 0 \\ \frac{1}{m_s} \\ 0 \\ \frac{-1}{m_u} \\ 0 \end{bmatrix} \quad \mathbf{F}=\begin{bmatrix} 0 & 0 \\ \frac{1}{m_s} & 0 \\ 0 & 0 \\ 0 & \frac{b_u}{m_u} \\ 0 & 1 \end{bmatrix}$$

$$\mathbf{C}=\begin{bmatrix} -\frac{k_s}{m_s} & -\left(\frac{b_s+b_{sf}}{m_s}\right) & \frac{k_s}{m_s} & \frac{b_s}{m_s} & 0 \\ \frac{k_s}{m_u} & \frac{b_s}{m_u} & -\left(\frac{k_s+k_u}{m_u}\right) & -\left(\frac{b_s+b_u}{m_u}\right) & \frac{k_u}{m_u} \\ 1 & 0 & 0 & 0 & 0 \\ 0 & 1 & 0 & 0 & 0 \\ 0 & 0 & 1 & 0 & 0 \\ 0 & 0 & 0 & 1 & 0 \\ 0 & 0 & 0 & 0 & 1 \\ 0 & 0 & -k_u & -b_u & k_u \\ -k_s & -b_s & k_s & b_s & 0 \end{bmatrix} \quad \mathbf{D}=\begin{bmatrix} \frac{1}{m_s} \\ \frac{-1}{m_u} \\ 0 \\ 0 \\ 0 \\ 0 \\ 0 \\ 0 \\ 0 \end{bmatrix} \quad \mathbf{E}=\begin{bmatrix} \frac{1}{m_s} & 0 \\ 0 & \frac{b_u}{m_u} \\ 0 & 0 \\ 0 & 0 \\ 0 & 0 \\ 0 & 0 \\ 0 & 0 \\ 0 & 0 \\ 0 & b_u \\ 0 & 0 \end{bmatrix}$$